Developing a tile drainage module for Cold Regions Hydrological Model: Lessons from a farm in Southern Ontario, Canada

Mazda Kompanizare[*&#], Diogo Costa[+*], Merrin L. Macrae[&], John W. Pomeroy[*], Richard M. Petrone[&]

[*]Centre for Hydrology, University of Saskatchewan, Canmore and Saskatoon, Canada

[+]University of Évora, Mediterranean Institute for Agriculture, Environment and Development, Portugal

[&]University of Waterloo, Waterloo, Canada

[#]Corresponding author: kompanizare.mazda@usask.ca

Abstract

Systematic tile drainage is used extensively in agricultural lands to remove excess water and improve crop growth; however, tiles can also transfer nutrients from farmlands to downstream surface water bodies, leading to water quality problems. Thus, there is a need to simulate the hydrological behaviour of tile drains to understand the impacts of climate or land management change on agricultural runoff. The Cold Regions Hydrological Model (CRHM) is a physically based, modular modeling system developed for cold regions. Here, a tile drainage module is developed for CRHM. A multi-variable, multi-criteria model performance evaluation strategy was deployed to examine the ability of the module to capture tile discharge under both winter and summer conditions (NSE>0.29, RSR<0.84 and PBias <20 for tile flow and water table simulations). Initial model simulations run at a 15-min interval did not satisfactorily represent tile discharge; however, model simulations improved when the time step was lengthened to hourly but also with the explicit representation of capillary rise for moisture interactions between the rooting zone and groundwater, demonstrating the significance of capillary rise above the water table in the hydrology of tile drains in loam soils. Novel aspects of this module include the sub-daily time step, which is shorted than most existing models, and which may enable future water quality modules to be added, and the use of field capacity and its corresponding pressure head to provide estimates of drainable water and the thickness of the capillary fringe, rather using than detailed soil retention curves that may not always be available. An additional novel aspect is the demonstration that flows in some tile drain systems can be better represented and simulated when related to shallow water table dynamics.

Keywords: tile drainage, cold regions, hydrological model, capillary fringe, drainable water, water table fluctuations

1. Introduction

Harmful algal blooms and eutrophication in large freshwater lakes surrounded by agricultural lands are major environmental challenges in Canada and globally. The transport of nutrients, particularly phosphorus, in runoff from agricultural fields into rivers, ponds and eventually lakes is an important contributor to the increased frequency of algal blooms being experienced in North America and elsewhere (Sharpley et al., 1995; Correll, 1998; Filippelli, 2002; Ruttenberg, 2005; Schindler, 2006; Quinton et al., 2010; Costa et al., 2022). Nutrient transport from agricultural fields can occur via both surface runoff and tile drainage (Radcliffe et al., 2015), and recent increases in the frequency and magnitude of algal blooms in Lake Erie in North America have been attributed to tile drainage (King et al., 2015; Jarvie et al., 2017). Tile drain systems reduce the retention time of soil water, lessening waterlogging in fields and improving both crop growth and field trafficability for farmers (Cordeiro and Ranjan, 2012; Kokulan et al., 2019a). However, they are also important pathways for dissolved and particulate nutrients (Kladivko et al., 1999; Tomer et al., 2015). It has been estimated that 14% of farmlands in Canada (ICID, 2018) and 45% of fields in Southern Ontario, Canada (ICID, 2018; Kokulan, 2019) are drained by tile systems. In Alberta, tile drains have also been used to address salinity issues (Broughton and Jutras, 2013). Given their importance in hydrological budgets and biogeochemical transport, there is a need to understand the controlling mechanisms of water and nutrient export from tile systems as an integral part of the broader, modified hydrological system. The ability to integrate a dynamic quantification of tile drainage from fields in hydrological models can help understand the relative importance of this human-induced process as it interplays with an array of other phenomena, including energy and physical mass balance hydrological processes, climate change, and the impacts of modified land management practices on runoff and nutrient export.

There are several models that can represent tile drainage at the small basin scale, such as HYPE (Lindstrom et al., 2010; Arheimer et al., 2015), DRAINMOD (Skaggs, 1978, 1980a; Skaggs et al., 2012), MIKE SHE (Refsgaard and Storm, 1995) and SWAT (Arnold et al., 1998; Koch et al., 2013; Du et al., 2005; Du et al., 2006; Green et al., 2006; Kiesel et al., 2010). These models include conceptual components for many key hydrological processes, but research shows that they have been primarily designed and tested for temperate regions (Costa et al., 2020a). In Canada and other cold regions, some unique hydrological processes such as frozen soil, snowmelt, rain on snow, and runoff over and infiltration into frozen or partially-frozen soils may be very important (Rahman et al., 2014; Cordeiro et al., 2017; Pomeroy et al., 1998, 2007; Fang et al., 2010, 2013). Many hydrological processes, such as the sublimation of snow, energy balance snowmelt, and infiltration into frozen soils, are strongly affected by temperature and the phase changes of water, which make many existing models developed for warm regions less appropriate for regions with cold seasons (Pomeroy et al., 2007; Pomeroy et al., 2013; Pomeroy et al., 2016; Fang et al., 2010, 2013). Even for temperate regions, the representation of cold season processes is often underrepresented in models (Costa et al., 2020a).

Since the use of tile drainage is becoming popular in many cold regions, it has become important to integrate such human-induced process in specialized hydrological modelling tools for these regions, such as the Cold Regions Hydrological Modelling platform (CRHM, Pomeroy et al., 2007; 2013; 2022). CRHM was initially developed in 1998 to assemble and explore the hydrological understanding developed from a series of research basins spanning Canada and elsewhere into a flexible, modular, object-oriented, multiphysics platform for simulating hydrological processes and basin response in cold regions (Pomeroy et al., 2007; 2022). The modular CRHM platform allows for multiple representations of forcing data interpolation and extrapolation, hydrological model spatial and physical process structure and parameter values. Many existing models typically operate at default daily or monthly time intervals, which is inadequate for the prediction of many short-duration "flashy" hydraulic responses often observed in tiles (Pluer et al., 2020; Vivekananthan, 2019; Vivekananthan et al., 2019; Lam et al., 2016a, 2016b; Macrae et al., 2019). Indeed, the ability to simulate shorter time intervals (e.g., hourly) facilitates the ability to capture both the rising and falling limbs of tile flow hydrographs, as well as the magnitude of peak flows, both of which are important to tile drain chemistry and export (Rozemeijer et al., 2016; Williams et al., 2015, 2016; Macrae et al., 2019).

Hydrological process models such as DRAINMOD, MIKE SHE and SWAT use a combination of empirical and physically based formulations for the simulation of tile flow derived by Hooghoudt (1940), Kirkham (1957), van Schilfgaarde (1974), Bouwer and van Schilfgaarde (1963) and Skaggs et al., (1978). Such formulations contemplate both cases where the water table is below and above the ground surface (Kirkham, 1957). In contrast, simulations of tile drainage in other models such as HYPE use empirically derived recession curves (Eckersten et al., 1994) to simulate tile flow and soil hydrological storage (typically represented as water table). In cases where there is a need for more focus on soil matrix hydrology and less need for understanding hydrological processes at the catchment scale and the relative contribution of tiles (and its interplay), modellers tend to use specialised porous-media PDE-based (partial differential equation-based) numerical models such as HYDRUS (Simunek et al., 2011) and MACRO (Larsbo and Jarvis, 2003).

The amount of water transported by tiles depends on soil moisture dynamics and the positioning of the water table, which are in turn affected by many factors, including soil type, surface topography and morphology, as well as the local climate and the hydrological characteristics of the field (Frey et al. 2016; Klaiber et al., 2020; Coelho et al., 2012; King et al., 2015). Thus, to provide reliable estimations of water loss from farmland via surface runoff and tile flow, models must be able to predict soil moisture storage and the water table elevation accurately (Brockley, 1976; Rozemeijer et al., 2016; Javani-Jouni et al., 2018). Many studies have shown that in some soil types, including silty loam and clay loam soils, the drainable water is less than expected based on the effective porosity (*e.g.*, Skeggs et al., 1978; Raats and

Gardner, 1974). Raats and Gardner (1974) have argued that the calculation of drainable porosity requires knowledge of water table elevation and the distribution of soil moisture above the water table. Skaggs et al. (1978) added that the calculation of drainable porosity should consider "the unsaturated zone drained to equilibrium with the water table". However, because the soil column is often composed of different soil layers with varying physical characteristics, drainable porosity varies with evapotranspiration rate, soil water dynamics and the depth of saturated water (Logsdon et al., 2010; Moriasi et al., 2013). In a sandy loam soil, Lam et al. (2016a, 2016b) demonstrated that tile drainage was not initiated until soil was at or above field capacity. Williams et al. (2019) observed in the American Midwest that tile drainage was not initiated until the field storage capacity had been exceeded. It has also been shown that despite the presence of tile drains, the soil above the tile may not always drain all gravitational water following a rainfall/snowmelt event and the soil may remain at or above field capacity (Skaggs et al., 1978; Lam et al., 2016a). Therefore, the soil drainable water content may be considerably smaller than the storage capacity. This is related to matric potential within the vadose zone, which is driven by the soil characteristics but can also be due to the development of a capillary fringe that reduces the rate of vertical percolation through the unsaturated zone, reducing tile flow (Youngs, 2012). Despite this evidence, some saturated flow models that simulate tile flow overlook the effect of capillary rise and over-estimate the soil drainable water. Other models that represent unsaturated flow (i.e., HYDRUS 3D, Simunek et al., 2011) using Richard's Equation (Richards, 1931) capture the effect of capillary rise and saturation-pressure variation within the soil profile and assess the soil drainable water more accurately. Although the effect of capillary rise is considered in DRAINMOD through the concept of drainable porosity (represented as a "water yield") (Skaggs, 1980b), and is calculated for layered soil profiles (Badr,1978), it requires detailed information surrounding the soil water characteristic curve (Skaggs, 1980b). Although it is indeed optimal to use soil-specific water characteristic curves, Twarakawi et al. (2009) found that it was possible to employ average representative values from the soil water characteristic curve to represent soil drainable water where a soil-specific curve was not available. They found in this case that the model performance was reduced.

In this study, a new Tile Drainage Module (TDM) was developed and incorporated within the physically based, modular Cold Regions Hydrological Modelling (CRHM) platform (Pomeroy et al., 2022) to enable hydrological simulations in tile-drained farm fields in cold agricultural regions. As a first iteration, the new module was developed for a field with sloping ground and loam soil with imperfect drainage. Such landscapes are common in the Great Lakes Region (e.g., Michigan and Vermont, USA and Ontario, Canada) and tile drainage in such landscapes has not been as widely studied as it has been in clay-dominated soil. In this module, considerations were explicitly included for the effects of capillary rise and annual groundwater water table fluctuations on drainable soil water storage. The use of field capacity and groundwater/soil water elevation head (Twarakawi et al., 2009) to modulate soil drainable water across the soil profile, including the capillary fringe region, is an innovative aspect of the model that has been demonstrated to circumvent the need for water characteristic curves. The development of this physically based module provides insight into hydrological processes in tile drainage from sloping landscapes with imperfect drainage, which are increasingly being artificially drained.

2. Materials and Methods

2.1 Study area

The study site is a ~10 ha farm field located near Londesborough, Ontario at UTM 17T 466689m E, 4832203m N, shown as LON in Fig. 1a. Mean annual precipitation recorded in this region is 1247 mm (ECCC, 2020). Mean air temperature is 7.2 ^{o}C, with annual maxima in July (25.9 ^{o}C) and minima in January (-10.2 ^{o}C), (ECCC, 2020). Soil texture has been identified as Perth clay loam (Gr. Br. Luvisolic), with a slope between 0.2 and 3.5%. The field is systematically drained with a tile depth of 0.9 m and a spacing of 14 m (laterals). The tile network collects infiltrated water from about 75% of the field (~ 7.6 ha) but may also receive lateral groundwater flow from neighbouring fields. Water yields from the tile drain laterals (10 cm diameter) are discharged via a common tile outlet (main, 15 cm diameter) below ground. Surface runoff from the field is directed toward a common outlet on the surface using plywood berms installed along the field edge (see van Esbroeck et al., 2016). The tile and surface runoff outlets do not join into a common outlet and are fully separated from one another, even during surface ponding events. The field is a corn-soy-winter wheat rotation with cover drops and rotational conservation till (shallow vertical tillage every three years). Additional details related to farming practices are provided in Plach et al. (2019), soil characteristics are provided in Plach et al. (2018a) and Plach et al. (2018b) and equipment and monitoring are provided in van Esbroeck et al., (2016). The outlets for both surface and tile flow are located at the edge of the field and drain into an adjacent field (Fig. 1b). Water tends to accumulate in a topographic low in the field, in front of the field outlet during snowmelt or high-intensity rainfall events, presumably due to either surface runoff or return flow (see ponded area, Fig. 1b). However, surface water or elevated soil moisture conditions are not observed in this topographic low during smaller events or dry periods of the year, suggesting that this saturated ponding is not in a perennial groundwater discharge zone. Although surface ponding is observed in the topographic depression within the field, water discharges freely at the opposite end of the culvert, facilitating the measurement of flow.

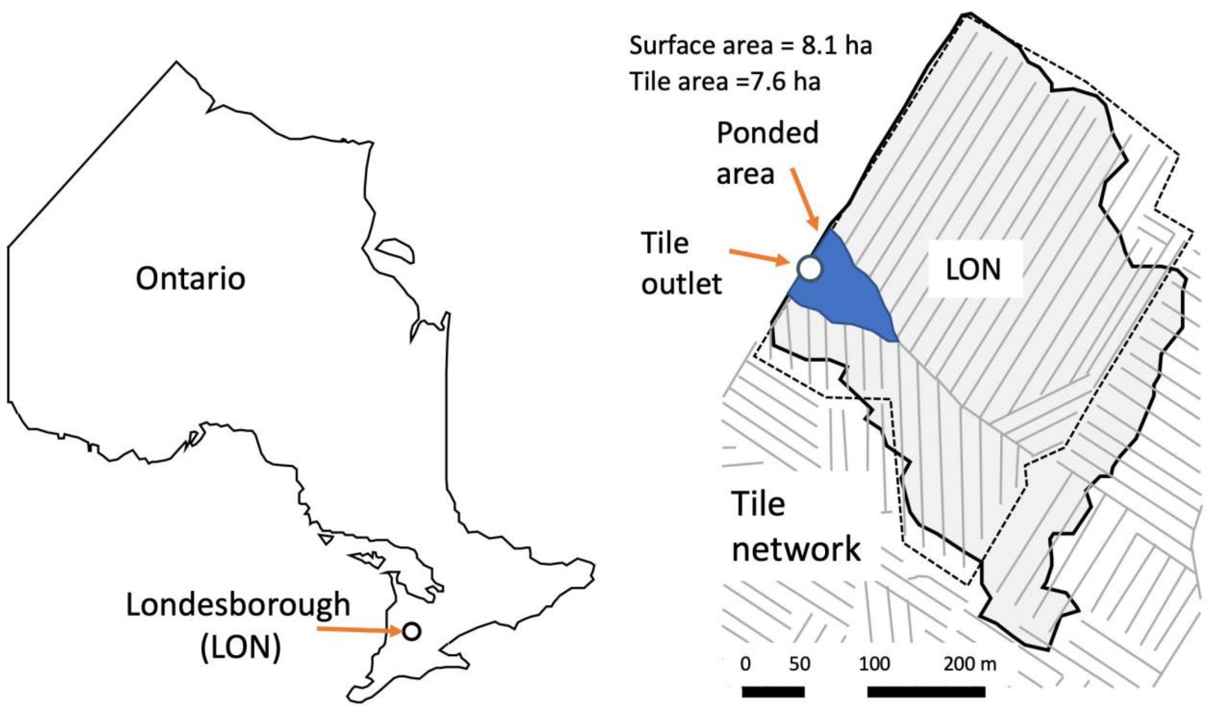

a) b)

b) Figure 1. (a) Location of the study area in South of Ontario and the (b) Londesborough (LON) farm with its tile network.

2.2 CRHM: The modelling platform

The modular CRHM platform includes options for empirical and physically based calculations of precipitation phase, snow redistribution by wind, snow interception, sublimation, sub-canopy radiation, snowmelt, infiltration into frozen and unfrozen soils, hillslope water movement, actual evapotranspiration, wetland fill and spill, soil water movement, groundwater flow and streamflow (Pomeroy et al., 2007; 2022). Where appropriate, it calculates runoff from rainfall and snowmelt as generated by infiltration excess and/or saturated overland flow, flow over partially frozen soils, detention flow, shallow subsurface flow, preferential flow through macropores and groundwater flow. Water quality can also be simulated in CRHM (Costa et al., 2021). Modules of a CRHM model can be customized to basin setup, such as delineating and discretizing the basin, conditioning observations for extrapolation and interpolation in the basin, or are process-support algorithms such as for estimating longwave radiation, complex terrain wind flow, or albedo dynamics, but most modules commonly address hydrological processes such as evapotranspiration, infiltration, snowmelt, and streamflow discharge. CRHM discretizes basins into hydrological response units (HRU) for mass and energy balance calculations, each with unique process representations, parameters, and position along flow pathways in the basin. HRU are connected by blowing snow, surface, subsurface and groundwater flow and together generate streamflow which is routed to the basin outlet. The size of TDM HRUs is flexible and can be as small as the size of a single tile pipe (e.g., 1 m) times the pipe spacing (which was 14 m in our case study region), and as large as entire tile networks within a given farm or study area. CRHM does not require a stream within a modelled basin. The feature allows CRHM to model the hydrology of cold regions dominated by storage and episodic runoff, such as agricultural fields.

Although CRHM has the capability to represent many hydrological and thermodynamic processes, not all processes need/must be represented in all situations. The modular design of the CRHM platform enables the user to activate or inactive specific processes to optimize the model for a particular situation. This is a modelling approach that enables testing different modelling hypotheses and has been pioneered by CRHM and other models, which has inspired a range of hydrological (e.g., SUMMA, Clark et al., 2015a, 2015b), hydrodynamic (e.g., mizuRoute, Mizukami et al., 2015) and biogeochemical (e.g., OpenWQ, Costa et al., 2023a, 2023b) modelling tools. For example, in the current study, blowing snow was not employed in CRHM as it does not appear to be significant at the study site (periodic snow surveys showed relatively uniform snow cover). Preferential flow into tile drains was not developed for the current simulation as although it is a key process in clay loam soil, as it does not appear to be a significant driver of preferential flow into tile drains in coarse textured soil (Pluer et al., 2020; Macrae et al., 2019). Freeze-thaw processes in soil were also not employed here as there is very little seasonal soil frost in the temperate Great Lakes region due to the persistent snow cover, and where soil frost occurs, it is restricted to brief periods and shallow depths (above 10 cm depth) (Macrae unpublished data).

2.3 Observations and input data for the model

Tile flow, water table elevation (water table elevation head) and surface flow were measured at the site between Oct. 2011 and Sept. 2018 at 15-minute intervals. It was not possible to install more than one measuring station for water table elevation and soil moisture at the site due to farming activity; consequently, water table elevation head and soil moisture were measured at the approximate midpoint of the field at the edge-of-field. Both tile flow rates and surface runoff were determined using simultaneous measurements of flow velocity and water depths in each of the pipes at the edge-of-field using Hach Flo-tote sensors and an FL900 data logger (Onset Ltd.) (Table A1, Appendix A). Continuous measurements of velocity were included due to the potential for impeded drainage under very wet conditions or caused by the accumulation of snow and ice around the surface culvert in winter. An additional barometrically-corrected pressure transducer (U20, Onset Ltd.) (Table A1) was also used for periods when the flow sensors did not function using a rating curve developed from the depth-velocity sensors. The water table elevation was measured using a barometric pressure-corrected pressure transducer (U20, Onset Ltd.).

Air temperature, wind speed, air relative humidity, incoming solar irradiance and rainfall were also measured at the site at 15-minute intervals and used to force the model. Variable names and their symbols in CRHM are listed in Appendix B. The air temperature, wind speed and incoming solar radiance measurements were collected 1 m above ground using a Temperature Smart Sensor S-THB-M002, Wind Smart Sensor Set S-WSET-M002 and a Solar Radiation Sensor (Table A1). Rainfall and relative humidity were measured via a tipping bucket rain gauge (Table A1) and an RH Smart Sensor (Table A1). These observations were continuously recorded throughout the study period, except for brief periods of instrument failure and maintenance, when data from nearby stations (Table T1, Supplementary Material) was substituted using the double mass analysis method (Searcy and Hardison, 1960).

Although rainfall was recorded continuously at the field site, snowfall data was not. Snowfall data was obtained from nearby stations (Wroxeter-Davis and Wroxeter, Environment Canada, 2021), located 31.7 km from the field site. Periodic snow surveys done at the site throughout the study period found that data from the nearby stations was a close approximation of snow at the field site (Plach et al., 2019). Hourly snowfall observations from Wroxeter-Geonor were used for the period between 2015 and 2018, whereas daily data from the Wroxeter-Geonor were used for the 2011 to 2014 period, reconstructed to hourly snowfall time series based on the method presented by Waichler and Wigmosta (2003).

2.4 Development of the new tile module

A Tile Drainage Module (TDM) was developed within CRHM (Figures 2, 3) with the goal of adding the ability to simulate tile flow and the resulting saturated storage (water table) at an hourly time step. CRHM was forced with hourly precipitation, air temperature, solar radiation, wind speed and relative humidity to calculate hydrological states and fluxes in HRUs and the basin. The model requires parameterizations that specify the hydraulic and hydrological properties of the soil, including its thickness, saturated hydraulic conductivity (K), and surface cover. CRHM calculates water storage and fluxes between HRUs, as well as vertical fluxes amongst different hydrological compartments (within each HRU) that include snow, depressional storage, different soil layers, and groundwater.

Using the simulation of soil moisture (including both saturated and unsaturated soil moisture) performed by the original CRHM "*Soil*" module, TDM calculates the dynamic tile flow rate that, in turn, feeds back to soil moisture at each time step. The presence of a capillary fringe (sometimes referred to as the tension-saturated zone within the soil profile) and its effects are considered by limiting the amount of drainable soil water. TDM uses site-specific information regarding the tile network, such as tile depth, diameter and spacing. Information regarding site-specific details regarding tile depth, diameter and spacing may be obtained directly from landowners or can be estimated based on standard design and installation guidelines for the region. This information was used to set up the model together with parameterization to translate the hydrological effects of the soil capillary fringe (CF), if present, through two variables, CF thickness and CF drainable water (discussed in Section 2.5, Figures 2, 3). These two variables are used to limit the fraction of the soil moisture that can freely drain to the tiles.

2.4.1 Soil moisture and water table elevation

The TDM uses the water quality soil module or soil module (*WQ_soil* or *Soil*), which divides the soil column into two layers: a recharge layer where evapotranspiration and root uptake generally take place and a deeper layer that connects to the groundwater system. Since CRHM's state variable for soil moisture is soil water storage volume (Fig. 2), the model results were converted into water table elevation above the semi-permeable layer (Table B1, Appendix B; see Fig. 2b for comparison with water table observations) by dividing volumetric soil moisture content (Table B1) by soil porosity (Table B1) for the cases with no capillary fringe above the water table. Additional steps were taken for periods when a capillary fringe developed (discussed below).

2.4.2 Capillary fringe and drainable water

Soil moisture in the capillary fringe is equal to the average volumetric water content at capillary fringe (θ_C) which is usually greater than the field capacity (θ_{fc}) (Bleam, 2017, Sect. 2.4). Therefore, while the positioning of the capillary fringe responds dynamically to the matric potential, the saturation profile within the capillary fringe remains constant, as well as its thickness because it only depends on the pressure head (capillary forces) that are related to the grain size distribution and field capacity (h_{fc}) as introduced by Twarakawi et al. (2009). Therefore, the drainable water in the capillary fringe becomes the difference between saturation (θ_s), computed dynamically in CRHM, and θ_C, which corresponds to the water held by capillary forces at the capillary fringe moisture content (Fig. 2). Accordingly, Fig. 2 shows the schematic soil characteristic curve for the three water level conditions contemplated in the model.

1. *Condition 1* is when the water table is at the surface and the soil is completely saturated (matric potential = 0);
2. *Condition 2* is when the water table drops but the upper boundary of the capillary fringe is at the soil surface; and
3. *Condition 3* is when the water table drops further, and the upper boundary of the capillary fringe drops beneath the surface.

In essence, the soil is completely saturated (θ_s) in *Condition 1*. Between *Conditions 1* and *2*, the capillary fringe occupies the entire soil column above the water level; thus, it can only release the volume of water corresponding to θ_s-θ_C or φ_c (dimensionless). Between *Conditions 2* and *3*, two layers with distinct hydraulic characteristics develop: (1) the top one at θ_{fc} that releases water up to θ_C-θ_{fc}, and (2) the lower one that corresponds to the capillary fringe and can release up to the volume of water corresponding to θ_s-θ_C or φ_c.

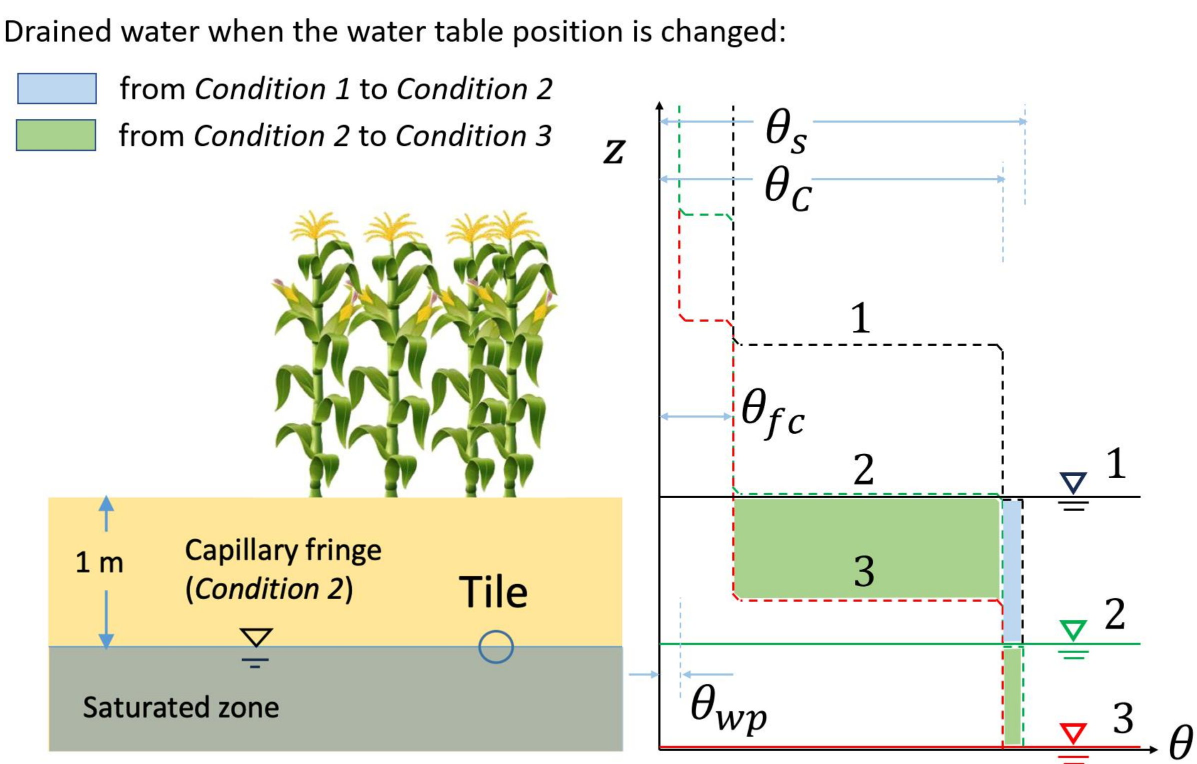

Figure 2. Schematic representation of the capillary fringe above the water table assuming a 1-m thickness (for demonstration purposes). The soil characteristic curves are shown for the three water level conditions considered: water level at the (1) surface, (2) intermediate depth, and (3) deeper depth. Two transitional drops can be seen in the characteristic curves, one from saturation (θ_s) to capillary fringe water content (θ_C) (between *Conditions 1* and *2*) and one from θ_C to field capacity (θ_{fc}) (between *Conditions 2* and *3*). The coloured areas (green and blue) of the right panel correspond to the amount of water that can be released between *Conditions 1* and *2* (blue) and between *Conditions 2* and *3* (green).

2.4.3 Tile flow calculation

A modified version of the Hooghoudt equation was used to calculate tile flow (Smedema et al., 2004), which presumes no surface ponding, an assumption that generally holds at the study site (Eq. 1), where water ponds only during very wet periods and on a small portion of the study site (see Fig. 1b). Hooghoudt's equation (Hooghoudt, 1940) is a steady state, physically based equation for saturated flow toward the tile drain. Flow estimates are provided based on the hydraulic conductivity of the soil and water table elevation above the tile pipe. It allows different saturated hydraulic conductivities for the layers above (AL) and below (BL) the tile (Fig. S1). At the study site, soil surveys have reported almost the same soil type (Loam) down to the depth of 90 cm (*e.g.*, Van Esbroeck et al., 2016; Plach et al., 2018b), which was parameterized in the model set up as,

$$q = \frac{8 \times K_2 \times d \times h}{L^2} + \frac{4 \times K_1 \times h^2}{L^2}, \qquad (1)$$

where K_1 and K_2 are respectively the saturated hydraulic conductivity in the upper and lower layers in mm h^{-1}; L is the tile spacing in mm; h is the water table elevation above the tile in mm,

d is the lower layer thickness in mm (Fig. S1), and q is the predicted tile flow in mm h^{-1}. The only variable that is dynamically updated by CRHM is h. Equation (1) is used to estimate the tile flow.

2.4.4 Calculation of the effect of tile flow on soil moisture and water levels

The simulated tile flows (see Sect. 2.3.3) are subtracted from the soil moisture. To calculate saturated storage (water table or groundwater elevation head level) from soil moisture calculated by the model, a threshold soil moisture content (sm_t) is defined, which consists of drainable water in the soil (φ_c) when the upper boundary of the capillary fringe is at the surface (*Condition 2*, Fig. 2) and was calculated as:

$$sm_t = sm_{max} - (C_t \times \varphi_c) \quad , \tag{2}$$

where sm_{max} is the maximum soil moisture and $C_t$is the capillary fringe thickness in mm. However, since the hydrological conditions of the soil are markedly different between the two transitional situations described in Sect. 2.3.2 and Fig. 2 (*Condition 1* to *2* and *Condition 2* to *3*), a step function was deployed for determination of the water table elevation:

$$WT = \begin{cases} \frac{sm_t - \left(C_t \times \left((\varphi_s - \varphi_c) + \theta_{fc}\right)\right)}{\varphi_s + \theta_{fc}} + \frac{sm - sm_t}{\varphi_c} & , if\ between\ Conditions\ 1\ and\ 2 \\ \frac{sm_{max}}{\varphi_s + \theta_{fc}} - \left(\left(\frac{sm_t - sm}{\varphi_s}\right) + C_t\right) & , if\ between\ Conditions\ 2\ and\ 3 \end{cases} , \tag{3}$$

where WT is water table elevation (or soil saturated storage, SSS) in mm from the bottom of the soil, and sm is soil moisture (both saturated and unsaturated storage) in the given time step in mm. Equation (3) is determined based on soil moisture curves in Fig. 2 and water level *Conditions 1-3* discussed in Sect. 2.3.2. In Fig. 2, the first and second parts of Eq. (3), which refer to *Conditions 1* to *2* and *2* to *3*, respectively, correspond to the volumes of soil water highlighted in "blue" and "green."

2.4.5 Lower semi-permeable soil layer and periodicity in annual groundwater levels

This model application focused on the study site field without including other adjacent areas. This was possible because years of field monitoring at this site have demonstrated that there is no observable surface flow into the site from adjacent farms. The tile network is restricted to the field and is not connected to tile drains or surface inlets in adjacent fields. However, field soil water table observations show evidence of annual groundwater level periodicity/fluctuation (Rust et al., 2019) that are sinusoidal in nature and cannot be neglected. Some studies predict the annual groundwater oscillations or the annual responses of groundwater to precipitation by using sine and cosine functions (De Ridder et al., 1974; Malzone et al., 2016; Qi et al., 2018). De Ridder et al. (1974) studied the design of the drainage systems and described the seasonal groundwater fluctuations observed in wells using sinusoidal curves. Malzone et al. (2016) used a sine function to predict annual groundwater fluctuations in the hyporheic zone. Qi et al. (2018) and Rust et al (2019) used a cross-wavelet transform, consisting of the superposition of sine and cosine curves, to predict shallow groundwater response to precipitation at the basin scale. This approach was used in this application to simulate annual fluctuations in groundwater water table, in Eq. (4), over a period of 1 year, with minimums around the middle of the growing season (mid-July), and maximums in the cold season (early February). This translates into the lower matric potential during the growing season, coinciding with soil moisture depletion, and then during the non-growing season, an elevated matric potential coinciding with an increase in the soil moisture, consistent with field observations. Thus, a sine function representing the annual fluctuations in percolation rate from soil to groundwater ($G_{y,i}$) layers in CRHM, through the lower soil semi-permeable layer (in mm hr^{-1}) is defined as:

$$G_{y,i} = \left[A \times sin\left(\frac{(T_s - D_d \times 24) \times 360}{24 \times 365.25}\right) - B\right] \times f_{y,i} \quad (4)$$

where T_s is the time step number, D_d is a time delay in days, A is the amplitude of the water table (WT) fluctuation, and B is an intercept factor. $f_{y,i}$ is a seasonal factor. The sine function coefficient (D_d, A, and B) and seasonal factor were adjusted for the whole period and for each year through model verification and shown in Table 1. Appendix C provides more details on the implementation of Eq. (4).

2.5 Model application and multi-variable, multi-metric validation

The study site is a relatively small field, and 2 HRUs were sufficient to capture its hydrological dynamics in CRHM. The HRUs represent (1) the area immediately upstream of the outlet where surface ponding occurs (depression storage); and (2) the remaining field (Fig. 3). The maximum ponding capacity of HRU 1 was estimated using the spatially distributed hydrodynamic model FLUXOS-OVERFLOW (Costa et al., 2016, 2020b). The CRHM model with its new TDM module were set up using the information described in Table 1. Soil textures at the LON site measured in a 25 m grid across three soil depths (0-25 cm, 25-50 cm, and 50-100 cm) averaged

29% sand, 48% silt, and 23% clay (Ontario Ministry of Agriculture, Food and Rural Affairs Soil Team, unpublished data). This soil grain size distribution corresponds with a soil saturated hydraulic conductivity of ~ 0.56 cm h^{-1} (~$10^{-2.5}$) (Garcia-Gutierrez et al., 2018), which was implemented in CRHM (0.5 cm h^{-1}), corresponding to a field capacity of 0.04 (volumetric water content) and h_{fc} of ~0.8 m (Twarskawi et al., 2009, based on a drainage flux of 0.1 cm d^{-1}).

A robust multi-variable, multi-metric model evaluation strategy was deployed to verify the capacity of the model to predict tile flow and its impact on the local hydrology. The outflows examined were tile flow, surface flow, and water table depth. The multi-metric approach contemplated five different methods, namely the Nash-Sutcliffe efficiency (NSE), Root-Mean-Square Error (RMSE), Model Bias (Bias), Percentage Bias (PBias), and RMSE-observation standard deviation ratio (RSR). See Appendix C for more details about the methodology used. It is generally assumed that NSE>0.50, $RSR \leq$ 0.70, and $PBias$ in the range of $\pm$25% are satisfactory for hydrological applications (Moriasi et al., 2007). Five different metrics were used to evaluate model accuracy in order to describe different aspects of the discrepancies between simulated and observed values. For example, Bias reveals the positive or negative general deviations of simulated values from the observed values, while RMSE shows the average absolute differences between them (Moriasi et al., 2007). Hourly values were used in these calculations, which departs from the daily and monthly analyses typically reported for these types of models. Although the hourly timestep is challenging for this sort of simulation, it is an important advance forward toward more detailed, accurate, and advanced models for tile drained agricultural fields. For example, Costa et al., (2021) noted that the successful extension of hydrological models to water quality studies relies on their ability to operate at small time scales in order to capture intense, short-duration storms that may have a disproportional impact on the runoff transport of some chemical species such as phosphorus – in essence, to capture hot spots and hot moments for flux generation.

Table 1. Key model parameters in CRHM for representation of the LON site.

Model Parameter	**Value**	**Unit**	**Source**	**Adjusted/Calibrated**	**Comment**
Soil depth or Soil thickness, T_{SL}	2	m		No	Assumed
Semipermeable layer depth	3	m		No	Assumed
Tile depth	0.9	m		No	Farmer/Blueprints of the field
Corn root depth	0.5	m		No	Online sources
Soil recharge zone thickness	0.5	m		No	Based on the root depth
Tile spacing	14	m		No	Farmer/Blueprints of the field
Soil porosity (soil drainable water) φ_S	0.045			Yes	Adjusted
Saturated Hydraulic conductivity, K in lower soil layer	5	mm h^{-1}		Yes	Adjusted
K in upper soil layer	5	mm h^{-1}		Yes	Adjusted
Capillary fringe thickness, T_{CF}	0.8	m		Yes	Adjusted
Capillary fringe drainable water, φ_C	0.03			Yes	Adjusted
Surface depression close to farm surface flow outlet (HRU2)	35	mm		Yes	Calculated
Surface depression in rest of the field (HRU1)	0	mm		No	Calculated

Surface area of HRU1	79000	m^2	No	Field observations and DEM
Surface area of HRU2	1000	m^2	No	Field observation and DEM
Soil module name in CRHM	WQ_soil		No	
Infiltration module name in CRHM	GreenAmpt		No	
Soil type in GreenAmpt module	5		Yes	Adjusted
Saturated K in GreenAmpt module	6	mm h^{-1}	Yes	Adjusted
Soil wilting point	0.025		Yes	Adjusted
A, in sine function	0.025	mm h^{-1}	Yes	Adjusted
B, in sine function	-0.005	mm h^{-1}	Yes	Adjusted
D_d, in sine function	15	d	Yes	Adjusted
$f_{2012,2}$ (Seasonal factor, sine function)	2.0		Yes	Adjusted
$f_{2015,2}$ (Seasonal factor, sine function)	1.8		Yes	Adjusted
$f_{2016,2}$ (Seasonal factor, sine function)	2		Yes	Adjusted
$f_{2017,2}$ (Seasonal factor, sine function)	1.4		Yes	Adjusted
$f_{y,i}$	1		No	By default for $y = 2012\ to\ 2017$ and $i = 1, 2$

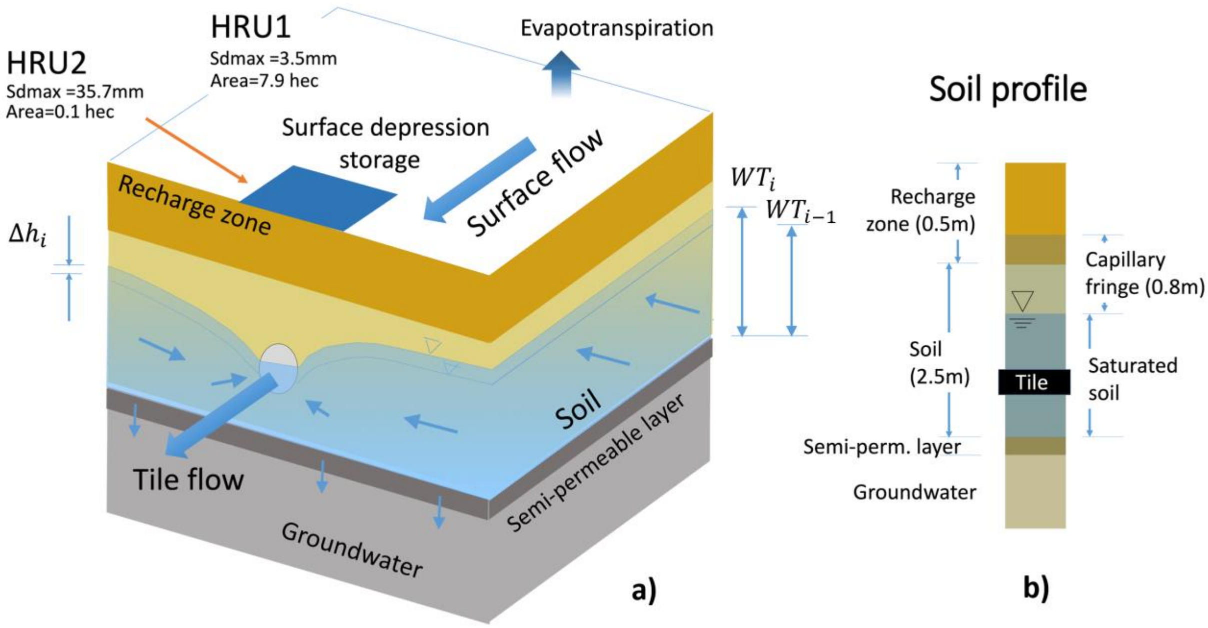

Figure 3. a) Schematic conceptual view of the CRHM model configuration, including soil layers, water table (WT), groundwater, and tile flow.; and b) soil profile, including the capillary fringe and its location relative to the soil and tile.

3. Results

3.1 Tile flow

The model was able to capture most tile flow events, both in terms of the timing and magnitude of peak flows and the most important seasonal patterns (Fig. 4). For example, the almost complete absence of tile flow during the growing season (May to September) was captured. The simulated flow peaks generally had a good agreement with observations, as well as the low flow or base flows during cold periods (December-March). The ascending and descending limbs of the response signal were also adequately predicted.

Results show that tile flows generally occurred during snowmelt events, as indicated by the synchrony between snow water equivalent (SWE) depletion and tile flow. The maximum snowpacks (or snow water equivalent, SWE) were markedly smaller during the winters of 2016 and 2017 when compared with those of 2013 to 2015. However, this did not necessarily translate into lower tile flows as precipitation also occurred as rain during these seasons. Although the magnitude of tile peaks was not always predicted accurately, the model was able to capture the annual trends of both an absence of tile flow during the summer months (growing season) and the ascending and descending limbs of the tile hydrograph during events (Figure 4).

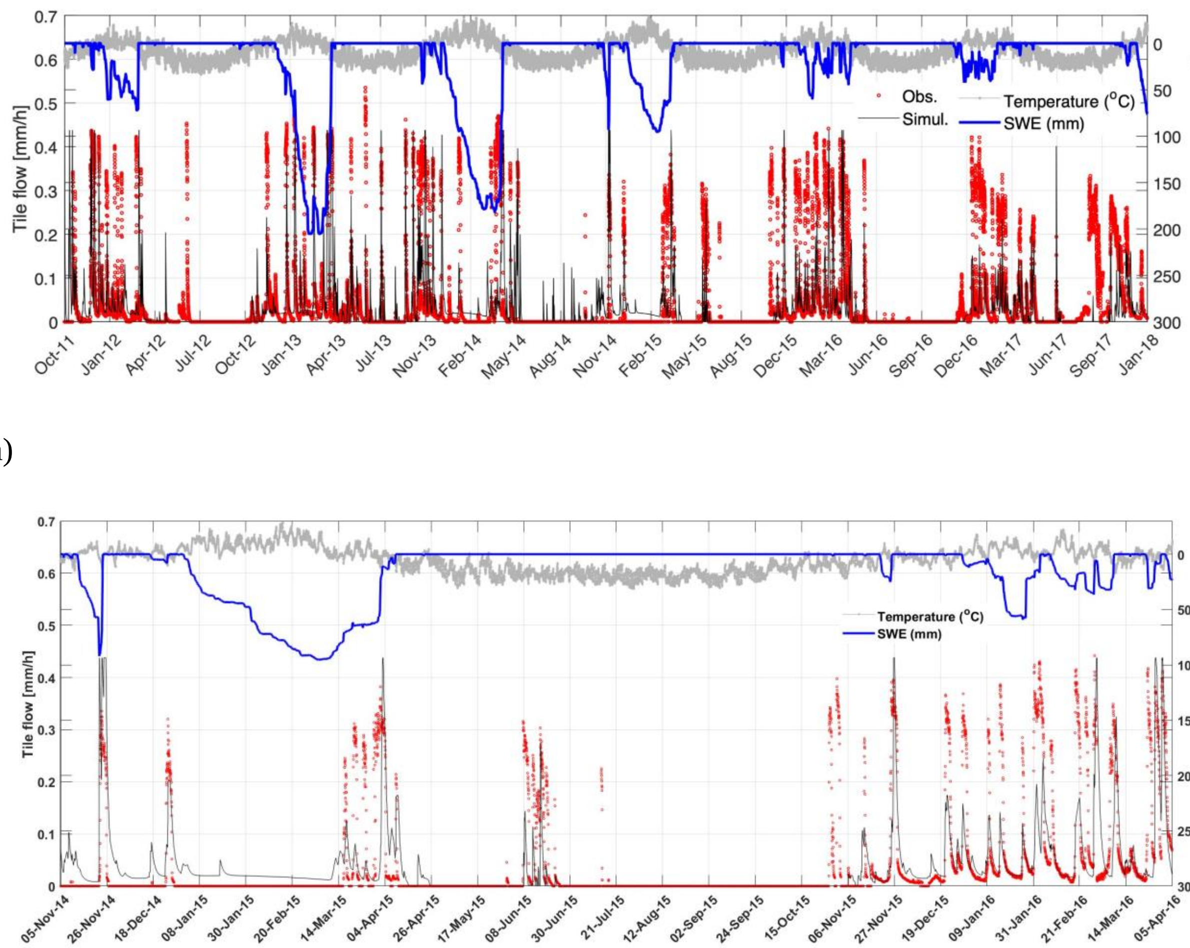

Figure 4. Comparison between observed and simulated tile flows, simulated SWE (snow water equivalent), and observed air temperature in the LON site, between October 2011 to January 2018 (a) and between November 2014 to April 2016 (b).

3.2 Water table or soil saturated storage

Simulated soil saturated storage and the observed water table are compared in Fig. 5, alongside air temperature and precipitation observations. Despite the gaps in the observational record during two periodic equipment failures, the model agrees well with observations. Above tile drains, water table fluctuations were controlled by infiltration/recharge, tile flow, groundwater flow, and matric potential that affect the drainable water from the capillary fringe. This caused flashier storage responses above the tile that were captured well by the model. In contrast, tiles did not withdraw water from the soil layer below the tile pipe and thus did not control water table fluctuations when levels were below the drain pipe, and tile drains did not flow during such periods. During the growing season, both the observed and simulated water table (or saturated storage) dropped abruptly because of the seasonal lowering of the regional groundwater water table. In the growing seasons of 2012, 2015 and 2016, which were dry years, large declines in the water table and saturated storage were observed, whereas in wetter years such as 2013 and 2014, seasonal water level declines were smaller. The seasonal declines in water level during the growing season led to a cessation in tile flow in most years (Fig. 4, 5), even following rainfall events. For example, there was a large precipitation event (~35 mm) in the growing season of 2016 that did not produce tile flow (apparent in both model and observations).

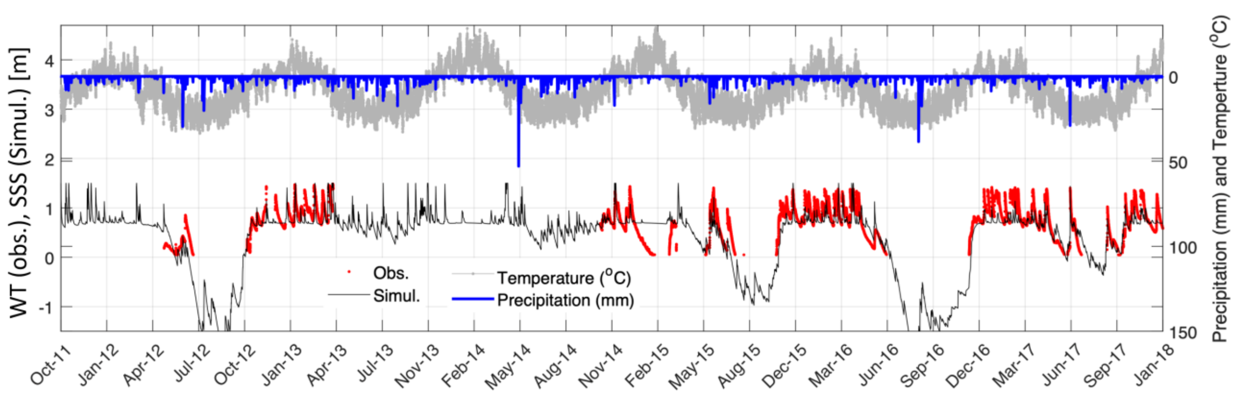

Figure 5. Time series of the simulated saturated storage and observed water table in the soil or groundwater layers of the model along with the observed temperature and precipitation. Given that tiles do not flow when the WT is below them, the WT = 0 when the water table elevation is at the depth of the tile drainpipe. In the figure, the water table is measured as the elevation above (+) or below (-) the tile pipe.

3.3 Surface flow and total flow

The model was not always able to capture the observed surface flow as satisfactorily as it captured tile drainage (Fig. 6a). Some possible reasons are uncertainties in the measurements of surface flow due to ponding in surface depressions on the field, which impeded the drainage of some of the surface runoff prior to when it exited the field through the culvert (see Fig. 1), or uncertainty in field estimates of SWE. However, the model performance improves considerably when both runoff and tile flow are combined (referred to as total flow, Fig. 6b). Indeed, most of the flow from the field was through tile drains (80% in 5-year average) rather than surface runoff (20% in 5-year average, Plach et al., 2019). The underestimation of both cumulative total and surface flows during 2017 and 2018 is possibly due to the removal of the blockage in the tile pipe in early 2017, which may have affected both surface and tile flow. The differences in timing of the simulated and observed surface flow for many of the main events (Figure 6) shows that there remain systematic issues in simulation of surface flow by CRHM which should be addressed in future research.

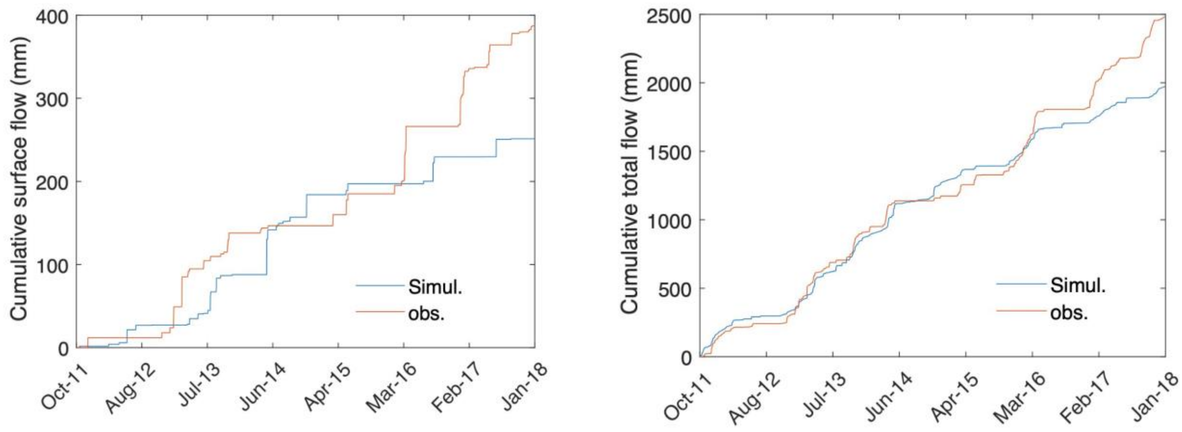

(a) (b)

Figure 6. Observed and simulated cumulative surface flow (a) and total flow (b).

3.4 Overall model performance

The model performance was calculated based on hourly data for various model outputs (Table 2). The results confirm that the model is robust in the sense that it can capture the main patterns of tile flow, surface flow, and water table elevation. The PBias values are below 25% for most of the fluxes and cumulative fluxes. The RSR values are also generally below 1.0. The NSE values are positive and above 0.3 for most fluxes, except for surface flow, where the model exhibited some difficulties. The weaker performance of the model in simulation of surface flow which is illustrated by the NSE coefficient can be partly related to difficulties in measurement of surface flow during flooding, ponding and freeze and thaw on the surface. The performance coefficients were calculated for May-September (Table 2b) and October-April (Table 2c). The results shows that surface flow biases are significantly larger and negative in May-September and are smaller and positive during October-April. For tile flow the Biases are a bit higher in May-September while for soil water table and total flow the biases are a bit lower in May-September. The NSEs are more acceptable in October to April for surface flow, tile flow and total flow but the NSE for WT is more acceptable in May-September.

Table 2. Performance coefficients for surface flow, tile flow and water table (WT/SSS), as well as total (tile + surface) flow, for the simulation period of October 2011 to January 2018. The coefficients were calculated for both hourly and daily flow rates, for the whole year (a) for May to September (b) and for October to April (c). (Green and red color show the seasonal coefficients improved and worsened, respectively, compared to their seasonal values).

a) Coefficients for whole year

Performance coefficients	**Surface flow**	**Tile flow**	**WT (m)**	**Total flow**	
NSE*	-2.29	0.31	0.49	-1.38	Coefficients calculated for hourly flow rates (mm h^{-1})
RMSE^	0.27	0.08	0.26	0.30	
Bias#	0.54	0.24	0.14	0.28	
PBias$	21.77	17.91	10.46	18.63	
RSR&	1.82	0.83	0.71	1.54	
NSE	-0.73	0.29	0.50	0.01	Coefficients calculated for daily flow rates (mm d^{-1})
RMSE	2.04	1.72	0.24	2.92	
Bias	0.35	0.20	0.09	0.22	
PBias	35.11	19.63	9.33	21.73	
RSR	1.31	0.84	0.70	0.99	

b) coefficients for May to September

Performance coefficients	**Surface flow**	**Tile flow**	**WT (m)**	**Total flow**	
NSE*	-18.98	0.19	0.40	-11.76	Coefficients calculated for hourly flow rates (mm h^{-1})
RMSE^	0.26	0.03	0.12	0.26	
Bias#	-1.43	0.49	0.03	0.11	
PBias$	-142.79	48.88	3.44	10.96	
RSR&	2.85	0.57	0.39	2.27	
NSE	-3.89	0.21	0.41	-1.08	Coefficients calculated for daily flow rates (mm d^{-1})
RMSE	1.39	0.73	0.11	1.66	
Bias	-1.43	0.49	0.02	0.11	
PBias	-142.79	48.88	2.07	10.96	

RSR	1.41	0.56	0.39	0.92

c) coefficients for October to April

Performance coefficients	**Surface flow**	**Tile flow**	**WT (m)**	**Total flow**	
NSE*	-0.37	0.24	0.20	-0.04	Coefficients calculated for hourly flow rates (mm h^{-1})
RMSE^	0.11	0.07	0.21	0.14	
Bias#	0.87	0.14	0.11	0.24	
PBias$	86.59	13.56	11.00	24.11	
RSR&	0.90	0.67	0.77	0.79	
NSE	-0.11	0.26	0.24	0.18	Coefficients calculated for daily flow rates (mm d^{-1})
RMSE	1.50	1.56	0.21	2.40	
Bias	0.87	0.14	0.11	0.24	
PBias	86.59	13.56	10.58	24.11	
RSR	0.81	0.67	0.75	0.70	

* Nash-Sutcliffe efficiency, ^Root-Mean-Square Error, #Model Bias, $Percentage Bias, &RMSE-observation standard deviation ratio

3.5 Presence of capillary fringe: effects and hypotheses

Results show that the thickness and vertical positioning of the capillary fringe have a strong impact on the amount of drainable soil water that can flow into tiles. To investigate this effect further, the response of tile flow and soil moisture to changes in the capillary fringe was examined. It should be noted that although this thickness may change slightly depending on the soil type and water retention curves (Skaggs et al., 1978), the model assumed a constant value given the field-scale nature of the simulations and myriad of processes contemplated. However, despite the simplification, the vertical positioning of the capillary fringe was still calculated and enabled a dynamic (time-dependent) calculation of the drainable soil water that was available for tile drainage over time.

Effect of capillary fringe on tile flow

Figure 7a relates the simulated normalized total cumulative tile flow (Q_{tR} , total tile flow divided by the total tile flow when there is no influence of capillary fringe) to capillary fringe drainable water ($\varphi_{cR} = \varphi_c/\varphi_s$) for two different φ_s values (0.045 and 0.125). The values were normalized (0 - 1 scale) for comparison purposes. As expected, the model indicates that tile flow increases with drainable water, but the relationship is non-linear, likely because as tile carrying capacity is exceeded more frequently, there is more opportunity for groundwater seepage and evapotranspiration. The direct effect of φ_s (comparing the solid and dashed lines) on tile flow is small because the amount of water that can effectively drain to the tile is controlled by the capillary fringe and the associated drainable soil water. Figure 7b looks at the impact of the capillary fringe thickness on tile flow. Here, the values are also normalized. Results show that Q_{tR} decreases with increasing normalized thickness of the capillary fringe, T_{CFR} ($\frac{T_{CF}}{D_t}$, capillary fringe thickness divided by tile depth), but only while the T_{CFR} is less than 1 that is when the capillary fringe position is above the tile but has not reached the soil surface. Beyond this point, increments in the capillary fringe thickness have no impact on tile flow because *Condition 1* has been reached (see Fig. 2), which essentially means that the capillary fringe has reached the soil surface. The match between the curves for two different φ_s values shows that the changes in φ_s does not influence the effect of normalized capillary fringe thickness and drainable water on normalized tile flow. In Appendix D the sensitivity of cumulative tile flow and mean soil water table elevation to different parameters are shown along with general approaches for evaluation of the model parameters for new sites, the site with no tile flow and water table observations.

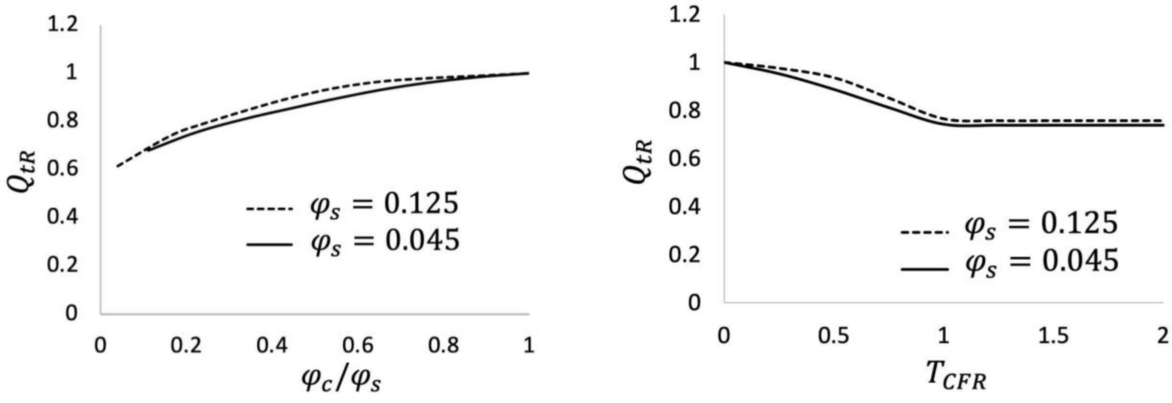

a) b)

Figure 7. Comparison between normalized tile flow (Q_{tR}) and (a) normalized drainable soil water (φ_c/φ_s) and capillary fringe thickness (T_{CFR}) for different maximum soil saturation values (φ_s), by drawing the model prediction lines.

Effect of capillary fringe on soil moisture

Observations and model results of WT reveal a bimodal frequency distribution (Fig. 8 and 9, respectively) with peaks at 0.85 m and 1.25 m depth, with the former corresponding to the depth of the tile pipe and the second peak reflecting capillary fringe thickness. In the simulated soil saturated storage (SSS as a measure of WT) frequency distributions (Fig. 9), the first peak highlights again the efficiency of the tile in removing soil moisture. In contrast, the second peak indicates a strong model response to differences in the capillary fringe thickness. It shows that when there is near-constant percolation from the bottom of the soil layer, the matric potential varies the greatest while it remains between the tile depth and the soil surface. While the water table fluctuates faster and is more unstable within this range, it also remains there for shorter periods. This bimodal response tends to push the water table depth below the tile. In Figure 9, we can see that the first peak happens at 0.9 m depth where the tile pipe is located, and the second peak happens at the depth equal to capillary fringe thickness. In Figure 9 the second peak is ore clear for the capillary fringe thickness of more than 1000 mm. The first peak in the observed water table frequency plot (Figure 8) happened around 0.8 m which almost matches with the tile depth. And the second peak happened at the depth of ~1.2 m which shows that the capillary fringe thickness should be around 1.2 m. But, to have a more reliable estimate for the capillary fringe, based on Figure 8, data is needed at depths greater than 1.5 m.

The bimodal behaviour of the observed water table and simulated saturated storage demonstrated here provides the opportunity to quantify the thickness of the capillary fringe using continuously monitored water table elevations. The capillary fringe thickness determined using this method can then be used as an input to the TDM module.

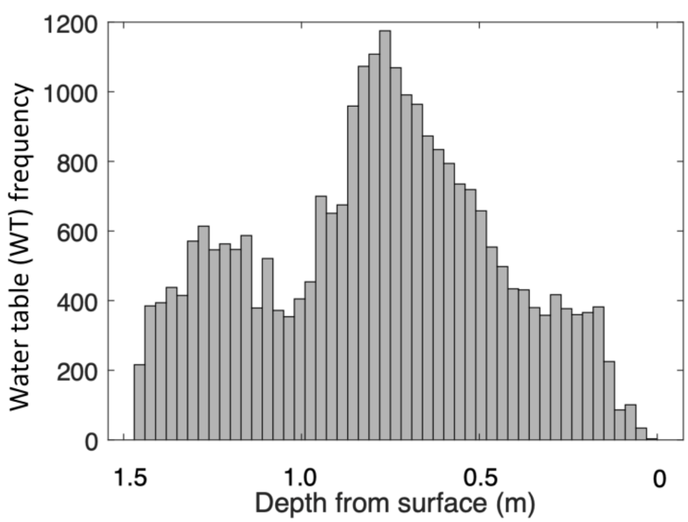

Figure 8. Histogram of the observed water table distribution for the period pf 2011 to 2018 in LON (Londesborough).

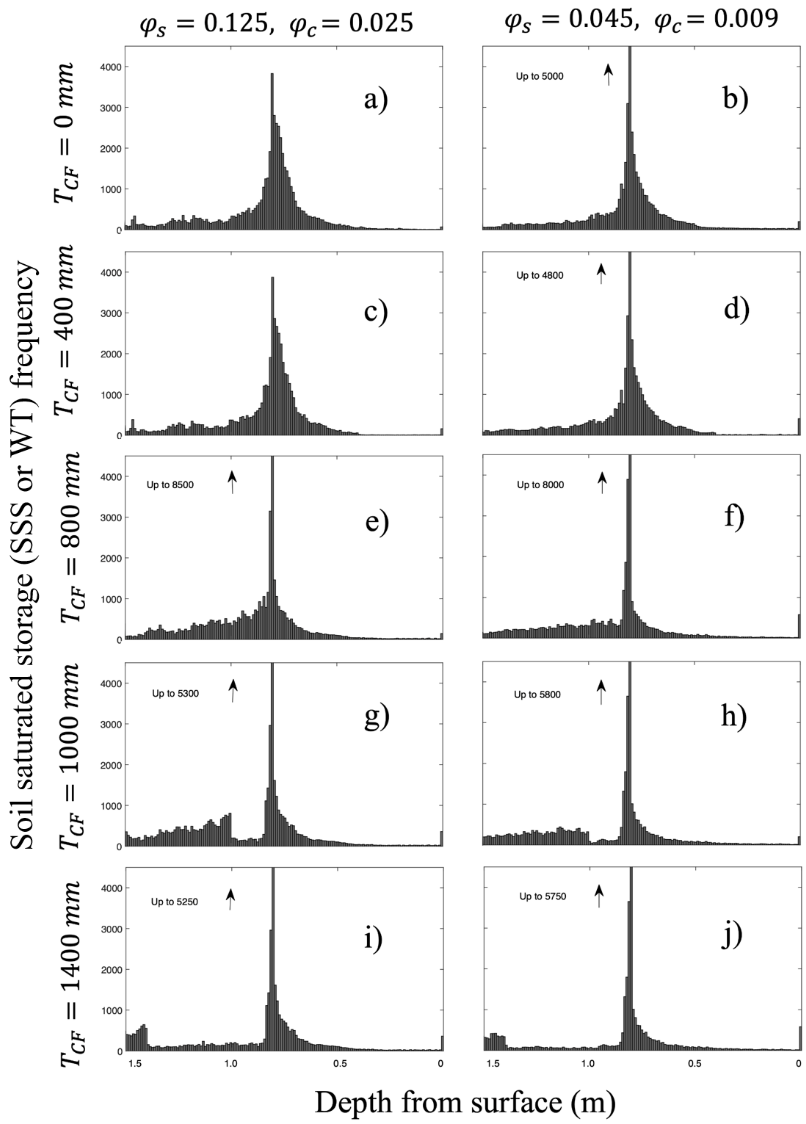

Figure 9. Histograms of the simulated soil saturated storages (SSS or WT) for the capillary fringe thicknesses of 0 (a,b), 400 (c,d), 800 (e,f), 1000 (g,h) and 1400 (i, j) mm and for the φ_s and φ_c of 0.125 and 0.025 (left column)as well as 0.045 and 0.009 (right column).

4. Discussion

4.1 Insights into key control mechanisms of tile flow for catchment-scale simulations

The model suggests that tile flow may not be accurately predicted exclusively based on the water table depth and soil saturated hydraulic conductivity as suggested by the steady-state flow assumptions of the Hooghoudt's equation (Hooghoudt, 1940). These results indicate two additional controls: (1) the amount of drainable soil water in the soil, which has also been identified in some field studies (*e.g.*, Skaggs et al., 1978; Moriasi et al., 2013) and (2) fluctuations in the groundwater table (GWRD) are important to account for in catchment-scale simulations. However, the relationship between drainable water and tile flow rates is non-linear, as demonstrated in Fig. 7a. This is because the residence time for groundwater seepage and evapotranspiration increases when the hydraulic tile carrying capacity is exceeded. Comparatively, the effect of soil drainable water, φ_s (see also Fig. 7a) on tile flow is small because the capillary fringe and associated drainable soil water control the amount of water that can effectively flow to the tile.

The verification of the model also indicated that the slopes of the rising and falling limbs of tile flow hydrographs and WT were very sensitive to (1) the ratio between K and drainable soil water; and (2) the net outflow in the soil through tile flow and groundwater level fluctuations (GWRD). This is supported by previous studies showing rapid responses of tile flow to precipitation events (Gentry et al., 2007; Smith et al., 2015) and others that have related rapid responses in tile discharge to antecedent moisture conditions (Macrae et al., 2007; Vidon and Cuadra, 2010; Lam et al., 2016a; Macrae et al., 2019), which can be affected by the development of a capillary fringe and its non-drainable water.

Results show that large fluctuations in WT (or SSS) and tile flow during the cold season, when the water table tends to be above the tile, are primarily triggered by the development of a capillary fringe that reduces the amount of drainable soil water. Model sensitivity tests showed that a small amount of drainable soil water produces steeper rising and falling responses (and with larger fluctuation amplitudes) in both the water table (saturated storage) and the tile flow. Indeed, this pattern can be observed by exploring differences in tile drain responses in clay loam soils with larger field capacities (and correspondingly smaller drainable water) and smaller hydraulic conductivity which are more likely to experience pronounced oscillations (*e.g.*, steeper rising and falling response curves) compared to tile drain responses of sandy soil, which is characterized by reduced capillary forces, lower field capacities (but correspondingly larger drainable water) and higher hydraulic conductivity. Notably, both model and observations of WT (as a proxy for soil moisture) reveal a bimodal (*i.e.*, two peaks) frequency distribution when examined in relation to the tile depth and capillary fringe thickness (Fig. 8 and 9, respectively). The two peaks (*i.e.* most frequently observed WT or SSS conditions) correspond with the (1) depth of the tile pipe (0.75 m), which demonstrates the efficacy of the tile at rapidly removing excess soil water, and the (2) the capillary fringe thickness (for the depths of 1.0 and 1.4 m, Figs. g, h, i and j) beyond which the amount of drainable water above the water table significantly increases.

These findings align well with studies such as Lam et al. (2016a) that recorded soil moisture near saturation after tile flow had ceased, suggesting the development of a capillary fringe. Combined experimental and modeling works, such as in Moriasi et al. (2013) and Logsdon et al. (2010), also discuss the impact of drainable soil water (“drainable porosity” or “specific water yield”) on tile flow and note that the drainable water is, in turn, dependent on the soil type, soil-water dynamic and water table depth. However, these studies did not explore the dynamic nature of the capillary fringe and its thickness relative to the soil column above in determining the transient amount of drainage soil water that will impact the WT distribution and tile flow differently over time (*Conditions 1* to *3*, see Fig. 2). Herein, while a capillary fringe with a fixed thickness that is generally related to the soil properties was assumed, its vertical positioning was simulated dynamically, which allowed determining the drainable soil water based on the evolution of pressure head corresponding to field capacity. Thus, the development of the TDM has provided a step forward in the modeling of tile drainage and suggests that in loam soils such as those at the study site, the effects of a capillary fringe on tile flow should be included. Soil moisture (soil unsaturated storage) measurements from the study site by Van Esbroeck et al., (2017) between November 2011 and May 2014 from depths of 10, 30, and 50 cm (using EC-5 Soil Moisture Smart Sensor) showed that almost 90% of the gravitational soil moisture drains out with 0.5 to 2.5 h. It suggests that the water table and capillary fringe can reach an equilibrium condition within one hour at this field site, enabling us to use a steady state equation (Hooghoudt, 1940) to predict the dynamic behavior of the water table fluctuations.

4.2 Importance of capturing seasonal patterns in groundwater to improve tile flow predictions

The GWRD changed dramatically between seasons affecting soil moisture (both saturated and unsaturated storage of the soil) and tile flow patterns. Both observations and model results show that low precipitation and higher evapotranspiration rates tend to produce little tile flow during the growing season. These seasonal patterns in precipitation and evapotranspiration are accompanied by a reduction in soil moisture (both unsaturated storage and saturated storage) that leads to a substantial storage capacity in fields. Even following moderate and high-intensity storms during the growing season, rapid soil moisture increases are observed (both saturated and unsaturated soil storage); however, tile flow rarely develops, suggesting that the soil is able to hold the water (Lam et al., 2016a; Van Esbroeck et al., 2016). In contrast, tile flow is often observed during the cold season, even during smaller rainfall-runoff and snowmelt events because of reduced soil storage but also a seasonal increase in GWRD (Lam et al., 2016a; Macrae et al., 2007, 2019; Van Esbroeck et al., 2016). This concurs with several studies throughout the Great Lakes and St. Lawrence region that have reported stronger tile responses during the non-growing season, with the summer months often showing little to no tile flow (Lam et al., 2016a, 2016b; Jamieson et al., 2003; Macrae et al., 2007; Hirt et al., 2011; King et al., 2016; Van Esbroeck et al., 2016; Plach et al., 2019).

These results (the controlling effect of soil drainable water and groundwater level fluctuations on tile flow) suggest that while soil moisture (both saturated and unsaturated storage) is largely controlled by tile flow rather than GWRD in the cold season, this reverses in the growing season (*i.e.*, soil moisture controls tile flow), with soil moisture (both saturated and unsaturated storage) being also impacted by evapotranspiration. The controlling effect of groundwater fluctuations in the growing season has also been studied by Hansen et al., (2019). The model indicated that the rapid drops in observed WT during the growing season could not be explained by evapotranspiration alone as well as the crop root depths, thus pointing to the role of GWRD. Johnsen et al. (1995) and Akis (2016) also showed that the effect of groundwater accretion was more effective on tile flows than surface runoff. Also, Vaughan et al. (1999) found that tile drain flows in their study site in San Joaquin Valley of California were better explained and related to nonlocal groundwater appearance than to local variations in irrigation amount, evapotranspiration, variation in water storage or tile drain blockage. Thus, it was determined that in addition to soil saturated hydraulic conductivity and soil thickness, the seasonal groundwater fluctuations and capillary fringe drainable water are other important controlling factors on tile flow rates.

5. Conclusion

A new tile drain module within the modular Cold Regions Hydrological Modelling (CRHM) platform has been created and tested at the field scale to support the management of agricultural basins with seasonal snow covers. The model was tested and validated for a small working farm in southern Ontario, Canada, and presents a step forward in the dynamic simulation of tile flow and its effects on the hydrological cycle in cold climates. Observations and model results showed that the dynamic prediction of tile flow and soil moisture at catchment scales needs to account for (1) the amount of drainable soil water that can be affected by the development of a capillary fringe and (2) fluctuations in the groundwater water table, in addition to the typical (3) water table elevation above the tile pipe and (4) the soil saturated hydraulic conductivity considered by the steady-state flow Hooghoudt's equation.

The groundwater table and matric potential changed dramatically between seasons, affecting patterns of soil moisture and tile flow. Observations and model results showed that low precipitation and higher evapotranspiration rates caused minimal tile flows during the crop-growing season. Conversely, tile flow was often observed during the cold season, even during small rainfall-runoff and snowmelt events, due to a seasonal increase in the groundwater table and soil-saturated storage.

Model sensitivity tests showed that the capillary fringe strongly affected the amount of drainable soil water flowing into the tile. Tile flow increased with drainable water, but the relationship is highly non-linear likely because, as the tile carrying capacity is exceeded more frequently, there is more opportunity time for groundwater seepage and evapotranspiration. Finally, observations and model results reveal a bimodal soil-saturated storage response in the presence of tiles, which is controlled by the relative positioning of the capillary fringe in relation to the soil surface and the depth of tile drains below the soil surface. Capturing these dynamics is a critical advance enabling the accurate prediction of the swift hydrological changes caused by the presence of tiles in models.

The TDM was developed as a first approximation from a single field site. Given this limitation, it is not yet widely applicable across multiple field sites. However, the development of this module provides critical insights into its potential and performance for hourly time-step simulations, as well as the importance of regional groundwater table fluctuations and simplifying the capillary fringe parameters within models in some landscape types. Future work will include building on the model and adapting it for different soil textures, such as those in clay loam soils, where preferential flow can have a strong impact on soil-saturated storage and tile flow. Also, explicit representation of unsaturated flow will be needed to enable the use of the model regions where groundwater is disconnected from surface water, as commonly happens in arid and semi-arid regions. Subsequent steps include also the integration of the new TDM model with CRHM's water quality modules.

Code/Data availability

The tile flow and soil water table data are not publicly available and will be provided upon request to the data owner, Merrin Macrae. TDM code is not completely implemented in the main version of the Cold Regions Hydrological Model platform and is provided only upon request to the corresponding author.

Author contribution

MK and DC developed the model code and performed the simulations. MM prepared the data and supported the field work. MK, DC and MM prepared the manuscript with contributions from JP and RP. All authors edited the manuscript.

Competing interests

The contact author has declared that none of the authors has any competing interests.

Acknowledgements

Funding for this project was provided by the Canada First Excellence Research Fund's Global Water Futures programme through its Agricultural Water Futures project. Funding for the collection of the field data was provided by the Ontario Ministry of Agriculture, Food and Rural Affairs. The support of the Biogeochemistry Lab at the University of Waterloo for the collection of field data and of Tom Brown and Xing Fang of the Centre for Hydrology at the University of Saskatchewan for CRHM development and updates is gratefully acknowledged. The Maitland

Valley Conservation Authority is thanked for providing some precipitation, rainfall, and temperature data.

References

Akis R.: Simulation of Tile Drain Flows in an Alluvial Clayey Soil Using HYDRUS 1D, American-Eurasian J. Agric. & Environ. Sci., 16 (4), 801-813, https://doi.org/10.5829/idosi.aejaes.2016.16.4.12906, 2016.

Arheimer, B., Nilsson, J., and Lindstrom, G.: Experimenting with Coupled Hydro-Ecological Models to Explore Measure Plans and Water Quality Goals in a Semi-Enclosed Swedish Bay, Water, 7(7), 3906-3924, https://doi.org/10.3390/w7073906, 2015.

Arnold, J. G., Srinivasan, R., Muttiah, R. S., and Williams, J. R.: Large area hydrologic modeling and assessment part I: model development, J. Am. Water. Resour. Assoc., 34, 73-89, https://doi.org/10.1111/j.1752-1688.1998.tb05961.x, 1998.

Badr, A. W.: Physical properties of some North Carolina Organic Soils and the effect of land development on these properties, M.S. Thesis, Department of Biological and Agricultural Engineering, North Carolina State University, Raleigh, NC. 67 p., 1978.

Bleam, W. (2nd Edition): Soil and Environmental Chemistry, Academic Press, eBook ISBN: 9780128041956, 2017.

Bouwer, H. and van Schilfgaarde, J.: Simplified method of predicting the fall of water table in drained land, Trans. ASAE. 6(4), 288-291, 296, 1963.

Brockley, R. P.: The effect of nutrient and moisture on soil nutrient availability, nutrient uptake, tissue nutrient concentration, and growth of Douglas-Fir seedlings, Master Thesis, The University of British Columbia, 1976.

Broughton, R. and Jutras, P.: Farm Drainage. In the Canadian Encyclopedia, https://www.thecanadianencyclopedia.ca/en/article/farm-drainage/, last access: 14 February 2019.

Coelho, B. B., Murray, R., Lapen, D., Topp, E., and Bruin, A.: Phosphorus and sediment loading to surface waters from liquid swine manure application under different drainage and tillage practices, Agric. Water Manag., 104, 51-61, https://doi.org/10.1016/j.agwat.2011.10.020, 2012.

Cordeiro, M. R. C. and Ranjan, R. S.: Corn yield response to drainage and subirrigation in the Canadian Prairies, Trans. ASABE. 55(5), 1771-1780, https://doi.org/10.13031/2013.42369, 2012.

Cordeiro, M. R. C., Wilson, H. F., Vanrobaeys, J., Pomeroy, J. W., Fang, X., and The Red-Assiniboine Project Biophysical Modeling Team: Simulating cold-region hydrology in an intensively drained agricultural watershed in Manitoba, Canada, using the Cold Region

Hydrological Model, Hydrol. Earth Syst. Sci., 21, 3483-3506, https://doi.org/10.5194/hess-21-3483-2017, 2017.

Correll, D.: The role of phosphorus in the eutrophication of receiving waters: a review, J. Environ. Qual., 27, 261-266, https://doi.org/10.2134/jeq1998.00472425002700020004x, 1998.

Costa, D., Klenk, K., Knoben, W., Ireson, A., Spiteri, R., Clark, M.: A multi-chemistry modelling framework to enable flexible and reproducible water quality simulations in existing hydro-models: 1. The OpenWQ concept and the water quality modelling lab. ESS Open Archive. https://essopenarchive.org/doi/full/10.22541/essoar.168718167.75677635/v1, 2023

Costa, D., Klenk, K., Knoben, W.J.M., Ireson, A., Spiteri, R.J., Clark, M.P.: A multi-chemistry modelling framework to enable flexible and reproducible water quality simulations in existing hydro-models: 2. The OpenWQ-SUMMA and OpenWQ-CRHM model implementations and testing. ESS Open Archive. DOI:10.22541/essoar.168652285.59958331/v1, 2023.

Costa, D., Sutter, D., Shepherd, A., Jarvie, H., Wilson, H., Elliott, J., Liu, J., and Macrae, M.: Impact of climate change on catchment nutrient dynamics: insights from around the world. Environmental Reviews. **31**(1): 4-25. https://doi.org/10.1139/er-2021-0109, 2022

Costa, D., Baulch, H., Elliott, J., Pomeroy, J., and Wheater, H.: Modelling nutrient dynamics in cold agricultural catchments: A review, Environ. Model. Softw., 124, 104586, https://doi.org/10.1016/j.envsoft.2019.104586, 2020a.

Costa, D., Shook, K., Spence, C., Elliott, J., Baulch, H., Wilson, H., and Pomeroy, J.: Predicting variable contributing areas, hydrological connectivity, and solute transport pathways for a Canadian Prairie basin, Water Resour. Res., 56, 1-23, https://doi.org/10.1029/2020WR02798, 2020b.

Costa, D., Burlando, P., Liong, S.-Y.: Coupling spatially distributed river and groundwater transport models to investigate contaminant dynamics at river corridor scales. Environmental Modelling & Software, 86, 91–110. https://doi.org/10.1016/j.envsoft.2016.09.009, 2016

Costa, D., Pomeroy, J. W., Brown, T., Baulch, H., Elliott, J., and Macrae, M.: Advances in the simulation of nutrient dynamics in cold climate agricultural basins: Developing new nitrogen and phosphorus modules for the Cold Regions Hydrological Modelling Platform, J. Hydrol., 603, 1-17, https://doi.org/10.1016/j.jhydrol.2021.126901, 2021.

Clark, M. P., Nijssen, B., Lundquist, J. D., Kavetski, D., Rupp, D. E., Woods, R. A., Freer, J. E., Gutmann, E. D., Wood, A. W., Brekke, L. D., Arnold, J. R., Gochis, D. J., & Rasmussen, R. M. (2015). A unified approach for process-based hydrologic modeling: 1. Modeling concept. Water Resources Research, 51(4), 2498–2514. https://doi.org/https://doi.org/10.1002/2015WR017198

Clark, M. P., Nijssen, B., Lundquist, J. D., Kavetski, D., Rupp, D. E., Woods, R. A., Freer, J. E., Gutmann, E. D., Wood, A. W., Gochis, D. J., Rasmussen, R. M., Tarboton, D. G., Mahat, V., Flerchinger, G. N., & Marks, D. G. (2015). A unified approach for process-based hydrologic modeling: 2. Model implementation and case studies. Water Resources Research, 51(4), 2515–2542. https://doi.org/https://doi.org/10.1002/2015WR017200

De Ridder, N. A., Takes, C. A. P., van Someren, C. L., Bos, M. G., Messemaeckers van de Graaff, R. H., Bokkers, A. H. J., Stransky, J., Wiersma-Roche, M. F. L., and Beekman, T.: Drainage Principles and Applications. International Institute for Lan Reclamation and Improvement, P.O. Box 45 Wageningen The Netherlands, 1974.

Du, B., Arnold, J. G., Saleh, A., and Jaynes, D. B.: Development and application of SWAT to landscapes with tiles and potholes, Trans. ASAE, 48, 1121-1133, https://doi.org/10.13031/2013.18522, 2005.

Du, B., Saleh, A., Jaynes, D. B., and Arnold, J. G.: Evaluation of SWAT in simulating nitrate nitrogen and atrazine fates in a watershed with tiles and potholes, Trans. ASABE, 49, 949-959, https://doi.org/10.13031/2013.21746, 2006.

ECCC, Canadian Climate Normals 1981-2010 Station Data, https://climate.weather.gc.ca/climate_normals/results_1981_2010_e.html?searchType=stnProx&txtRadius=25&selCity=&selPark=&optProxType=custom&txtCentralLatDeg=43&txtCentralLatMin=41&txtCentralLatSec=55&txtCentralLongDeg=81&txtCentralLongMin=28&txtCentralLongSec=47&txtLatDecDeg=&txtLongDecDeg=&stnID=4545&dispBack=0, last access: 5 February 2020.

Eckersten, H., Jansson, P. -E., and Johnsson, H. (2nd edition): SOILN model-user's manual, Division of Agricultural Hydrotechnics Communications 94:4, Department of soil Sciences, Swedish University of Agricultural Sciences, 58pp, Uppsala, 1994.

Environment Canada, Canadian Climate Normals 1981-2010 Station Data, https://climate.weather.gc.ca/climate_data/daily_data_e.html?hlyRange=%7C&dlyRange=1966-06-01%7C2021-06-14&mlyRange=1966-01-01%7C2006-12-01&StationID=4603&Prov=ON&urlExtension=_e.html&searchType=stnName&optLimit=yearRange&StartYear=1840&EndYear=2022&selRowPerPage=25&Line=0&searchMethod=contains&Month=6&Day=4&txtStationName=Wroxeter&timeframe=2&Year=2021, last access: 10 May 2020.

Fang, X., Pomeroy, J. W., Westbrook, C. J., Guo, X., Minke, A. G., and Brown, T.: Prediction of snowmelt derived streamflow in a wetland dominated prairie basin, Hydrol. Erath Syst. Sci., 14, 991-1006, https://doi.org/10.5194/hess-14-991-2010, 2010.

Fang, X., Pomeroy, J. W., Ellis, C. R., MacDonald, M. K., DeBeer, C. M., and Brown, T.: Multi-variable evaluation of hydrological model predictions for a headwater basin in the Canadian Rocky Mountains, Hydrol. Earth Syst. Sci., 17, 1635-1659, https://doi.org/10.5194/hess-17-1635-2013, 2013.

Filippelli, G. M.: The global phosphorus cycle, Rev. Mineral. and Geochem., 48, 391-425, https://doi.org/10.2138/rmg.2002.48.10, 2002.

Frey, S. K., Hwang, H. T., Park, Y. J., Hussain, S. I., Gottschall, N., Edwards, M., and Lapen, D. R.: Dual permeability modeling of tile drain management influences on hydrologic and nutrient transport characteristics in macroporous soil, J. Hydrol., 535, 392-406, http://dx.doi.org/10.1016/j.jhydrol.2016.01.073, 2016.

Gentry, L. E., David, M. B., Royer, T. V., Mitchell, C. A., and Starks, K.: Phosphorus transport pathways to streams in tile-drained agricultural watersheds, J. Environ. Quality., 36, 408-415, https://doi.org/10.2134/jeq2006.0098, 2007.

Garcia-Gutierrez, C., Pachepsky, Y., and Martin, M. A.: Technical note: Saturated hydraulic conductivity and textural heterogeneity of soils, Hydrol. Earth Syst. Sci., 22, 3923-3932, https://doi.org/10.5194/hess-22-3923-2018, 2018.

Green, C. H., Tomer, M. D., Di Luzio, M., and Arnold, J. G.: Hydrologic evaluation of the Soil and Water Assessment Tool for large tile-drained watershed in Iowa, Trans. ASABE., 49, 413-422, https://doi.org/10.13031/2013.20415, 2006.

Hansen, A. L., Jakobsen, R., Refsgaard, J. C., Hojberg, A. L.,Iversen, B. V., and Kjaergaard, C.: Groundwater dynamics and effect of tile drainage on water flow across the redox interface in a Danish Weichsel till area, Advances in Water Resources, 123, 23-39, https://doi.org/10.1016/j.advwatres.2018.10.022, 2019.

Hirt, U., Wetzig, A., Amatya, M. D., and Matranga, M.: Impact of seasonality on artificial drainage discharge under temperate climate conditions, Int. Rev. Hydrobiol., 96, 561-577, https://doi.org/10.1002/iroh.201111274, 2011.

Hooghoudt, S. B.: Bijdrage tot de kennis van enige natuurkundige grootheden van de grand. Verslagen van Landbouwkundige Onderzoekingen, 46(7), 515-707, the Hague, The Netherlands (in Dutch), 1940.

ICID: World Drained Area-2018. International Commission on Irrigation and Drainage. http://www.icid.org/world-drained-area.pdf , last access: 14 February 2019.

Jamieson, A., Madramootoo, C. A., and Enright, P.: Phosphorus losses in surface and subsurface runoff from a snowmelt event on an agricultural field in Quebec, Can. Biosyst. Eng., 45, 11-17, 2003.

Jarvie, H. P., Johnson, L. T., Sharpley, A. N., Smith, D. R., Baker, D. B., Bruulsema, T. W., and Confesor, R.: Increased Soluble Phosphorus Loads to Lake Erie: Unintended Consequences of Conservation Practices?, J. Environ. Qual., 46, 123-132, https://doi.org/10.2134/jeq2016.07.0248, 2017.

Javani-Jouni, H., Liaghat, A., Hassanoghli, A., and Henk, R.: Managing controlled drainage in irrigated farmers' fields: A case study in the Moghan Plain, Iran, Agric. Water Manag., 208, 393-405, https://doi.org/10.1016/j.agwat.2018.06.037, 2018.

Johnsen, K. E., Liu, H. H., Dane, J. H., Ahuja, L. R., and Workman, S. R.: Simulating Fluctuating Water Tables and Tile Drainage with a Modified Root Zone Water Quality Model and a New Model WAFLOWM, Transactions of the ASAE, 38 (1), 75-83, https://doi.org/10.10031/2013.27814, 1995.

Kiesel, J., Fohrer, N., Schmalz, B., and White, M. J.: Incorporating landscape depressions and tile drainages of a northern German lowland catchment into a semi-distributed model, Hydrol. Process., 24, 1472-1486, https://doi.org/10.1002/hyp.7607, 2010.

King, K. W., Williams, M. R., Macrae, M. L., Fausey, N. R., Frankenberger, J., Smith, D. R., Kleinman, P. A. J., and Brown, L. C.: Phosphorus transport in agricultural subsurface drainage: A review, J. Environ. Qual., 44(2), 467-485, https://doi.org/10.2134/jeq2014.04.0163, 2015.

King, K. W., Williams, M. R., and Fausey, N. R.: Effect of crop type and season on nutrient leaching to tile drainage under a corn-soybean rotation, J. Soil and Water Conserv., 71, 56-68, https://doi.org/10.2489/jswc.71.1.56, 2016.

Kirkham, D.: Theory of land drainage, in, Drainage of Agricultural Lands. Agronomy Monograph, No. 7, American Society of Agronomy, Madison, Wisconsin, 1957.

Kladivko, E. J., Grochulska, J., Turco, R. F., Van Scoyoc, G. E., and Eigel, J. D.: Pesticide and nitrate transport into subsurface tile drains of different spacings, J. Environ. Qual., 28, 997-1004, https://doi.org/10.2134/jeq1999.00472425002800030033x, 1999.

Klaiber, L. B., Kramer, S. R., and Young, E. O.: Impacts of Tile Drainage on Phosphorus Losses from Edge-of-field Plots in the Lake Champlain Basin of New York, Water, 12, 328, https://doi.org/10.3390/w12020328, 2020.

Kock, S., Bauwe, A., and Lennartz, B.: Application of SWAT Model for a Tile-Drained Lowland Catchment in North-Eastern Germany on Subbasin Scale, Water Resour. Manage., 27, 791-805, https://doi.org/10.1007/s11269-012-0215-x, 2013.

Kokulan, V.: Environmental and Economic Consequences of Tile Drainage Systems in Canada, The Canadian Agri-Food Policy Institute (CAPI), 2019.

Kokulan, V., Macrae, M. L., Ali, G. A., and Lobb, D. A.: Hydroclimatic controls on runoff activation in a artificially drained, near-level vertisolic clay landscape in a Prairie climate, Hyrol. Process., 33, 602-615, https://doi.org/10.1002/hyp.13347, 2019a.

Lam, W. V., Macrae, M. L., English, M. C., O'Halloran, I. P., Plach, J. M., and Wang, Y.: Seasonal and event-based drives of runoff and phosphorus export through agricultural tile drains under sandy loam soil in a cool temperate region, Hydrol. Process., 30, 2644-2656, https://doi.org/10.1002/hyp.10871, 2016a.

Lam, W. V., Macrae, M. L., English, M. C., O'Halloran, I., and Wang, Y.: Effects of tillage practices on phosphorus transport in tile drain effluent in sandy loam agricultural soils in Ontario, Canada, J. Great Lakes Res., 42(6), 1260-1270, https://dx.doi.org/10.1016/j.jglr.2015.12.015, 2016b.

Larsbo, M., and Jarvis, N.: MACRO 5.0. A model of water flow and solute transport in microporous soil, Technical description. Swedish University of Agricultural Sciences, Division of Environmental Physics, Emergo 2003:6 Report, ISSN 1651-7210, ISBN 91-576-6592-3, 2003.

Lindstrom, G., Pers, C., Rosberg, J., Stromqvist, J., and Arheimer, B.: Development and testing of the HYPE (Hydrological Predictions for the Environment) water quality model for different scales, Hydrol. Res., 41(3-4), 295-319, https://doi.org/10.2166/nh.2010.007, 2010.

Logsdon, S. D., Schilling, K. E., Hernandez-Ramirez, G., Prueger, J. H., Hatfield, J. L., and Sauer, T. J.: Field estimation of specific yield in a central Iowa crop field, Hydrol. Process., 24, 1369-1377, https://doi.org/10.1002/hyp.7600, 2010.

Macrae, M. L., English, M. C., Schiff, S. L., and Stone, M. L.: Intra-annual variability in the contribution of tile drains to basin discharge and phosphorus export in a first order agricultural catchment, Agric. Water Manag., 92, 171-182, https://doi.org/10.1016/j.agwat.2007.05.015, 2007.

Macrae, M. L., Ali, G. A., King, K. W., Plach, J. M., Pluer, W. T., Williams, M., Morison, M. Q., and Tang, W.: Evaluating Hydrologic Response in Tile-Drained Landscapes: Implications for Phosphorus Transport, J. Environ. Qual., 48(5), 1347-1355, https://doi.org/10.2134/jeq2019.02.0060, 2019.

Malzone, J. M., Lowry, C. S., and Ward, A. S.: Response of the hyporheic zone to transient groundwater fluctuations on the annual and storm event time scales, Water Resour. Res., 52, 5301-5321, https://doi.org/10.1002/2015WR018056, 2016.

Mizukami, N., Clark, M. P., Sampson, K., Nijssen, B., Mao, Y., McMillan, H., Viger, R. J., Markstrom, S. L., Hay, L. E., Woods, R., Arnold, J. R., & Brekke, L. D. (2016). mizuRoute version 1: A river network routing tool for a continental domain water resources applications. Geoscientific Model Development, 9, 2223–2238. https://doi.org/10.5194/gmd-9-2223-2016

Moriasi, D. N., Arnold, J. G., Van Liew, M. W., Bingner, R. L., Harmel, R. D., and Veith, T. L.: Model Evaluation Guidelines for Systematic Quantification of Accuracy in Watershed Simulations, Trans. ASABE, 50(3), 885-900, https://doi.org/10.13031/2013.23153, 2007.

Moriasi, D. N., Gowda, P. H., Arnold, J. G., Mulla, D. J., Ale, S., Steiner, J. L., and Tomer, M. D.: Evaluation of the Hooghoudt and Kirkham Tile Drain Equations in the Soil and Water Assessment Tool to Simulate Tile Flow and Nitrate-Nitrogen, J. Environ. Qual., 42, 1699-1710, https://doi.org/10.2134/jeq2013.01.0018, 2013.

Plach, J. M., Macrae, M. L., Ali, G. A., Brunke, R. R., English, M. C., Ferguson, G., Lam, W. V., Lozier, T. M., McKague, K., O'Halloran, I. P., Opolko, G., and Van Esbroeck, C. J.: Supply and Transport Limitations on Phosphorus Losses from Agricultural Fields in the Lower Great Lakes Region, Canada, J. Environ. Qual., 47, 96-105, https://doi.org/10.2134/jeq2017.06.0234, 2018a.

Plach, J. M., Macrae, M. L., Williams, M. R., Lee, B. D., and King, K. W.: Dominant glacial landforms of the lower Great Lakes region exhibit different soil phosphorus chemistry and potential risk for phosphorus loss, J. Great Lakes Res., 44, 1057-1067, https://doi.org/10/1016/j.jglr.2018.07.005, 2018b.

Plach, J., Pluer, W., Macrae, M., Kompanizare, M., McKague, K., Carlow, R., and Brunke, R.: Agricultural Edge of Field Phosphorus Losses in Ontario, Canada: Importance of the Nongrowing Season in Cold Regions, J. Environ. Qual., 48, 813-821, https://doi.org/10.2134/jeq2018.11.0418, 2019.

Pluer, W. T., Macrae, M., Buckley, A., and Reid, K.: Contribution of preferential flow to tile drainage varies spatially and temporally, Vadose Zone J., 19: e20043, https://doi.org/10.1002/vzj2.20043, 2020.

Pomeroy, J. W., Gray, D. M., Shook, K. R., Toth, B., Essery, R. L. H., Pietroniro, A., and Hedstrom, N. R.: An evaluation of snow accumulation and ablation processes for land surface modelling, Hydrol. Process., 12, 2339-2367, https://doi.org/10.1002/(SICI)1099-1085(199812)12:15, 1998.

Pomeroy, J. W., Gray, D. M., Brown, T., Hedstrom, N. R., Quinton, W. L., Granger, R. J., and Carey, S. K.: The cold regions hydrological model: a platform for basing process representation and model structure on physical evidence, Hydrol. Process., 21, 2650-2667, https://doi.org/10.1002/hyp.6787, 2007.

Pomeroy, J. W., Fang, X., Shook, K., and Whitfield, P. H.: Predicting in Ungauged Basins Using Physical Principles Obtained Using the Deductive, Inductive, and Abductive Reasoning Approach, https://research-groups.usask.ca/hydrology/documents/pubs/papers/pomeroy_et_al_2003_3.pdf , 2013.

Pomeroy, J. W., Fang, X., and Marks, D. G.: The cold rain-on-snow event of June 2013 in the Canadian Rockies - characteristics and diagnosis, Hydrol. Process., 30, 2899-2914, https://doi.org/10.1002/hyp.10905, 2016.

Pomeroy, J. W., Brown, T., Fang, X., Shook, K. R., Pradhananga, D., Armstrong, R., Harder, P., Marsh, C., Costa, D., Krogh, S. A., Aubry-Wake, C., Annand, H., Lawford, P., He, Z., Kompanizare, M., and Lopez Moreno, J. I.: The cold regions hydrological modelling platform for hydrological diagnosis and prediction based on process understanding, J. of Hydrol., 615 (A), 128711, https://doi.org/10.1016/j.jhydrol.2022.128711, 2022.

Qi, P., Zhang, G., Xu, Y. J., Wang, L., Ding, C., and Cheng, C.: Assessing the Influence of Precipitation on Shallow Groundwater Table Response Using Combination of Singular Value Decomposition and Cross-Wavelet Approaches, Water, 10, 598, https://doi.org/10.3390/w10050598, 2018.

Quinton, J. G., Govers, G., van Oost, K., and Bardgett, R.: The impact of agricultural soil erosion on biochemical cycling, Nat. Geosci., 3, 311-314, https://doi.org/10.1038/ngeo838, 2010.

Raats, P. A. C. and Gardner, W. R.: Movement of water in saturated zone near a water table. Ch. 13 in Drainage for agriculture, J. van Schilfgraade, Ed., Agronomy Monograph. No. 17, American Society of Agronomy, Madison, WI, pp. 331-357, 1974.

Radcliffe, D. E., Reid, D. K., Blomback, K., Bolster, C. H., Collick, A. S., Easton, Z. M., Francesconi, W., Fuka, D. R., Johnsson, H., King, K., Larsbo, M., Youssef, M. A., Mulkey, A. S., Nelson, N. O., Persson, K., Ramirez-Avila, J. J., Schmieder, F., and Smith, D. R.: Applicability of Models to Predict Phosphorus Losses in Drained Fields: A Review, J. Environ. Qual., 44, 614-628, https://doi.org/10.2134/jeq2014.05.0220, 2015.

Rahman, M. M., Lin, Z., Jia, X., Steele, D. D., and DeSutter, T. M.: Impact of subsurface drainage on streamflows in Red River of the North basin, J. Hydrol., 511, 474-483, https://doi.org/10.1016/j.jhydrol.2014.01.070, 2014.

Refsgaard, J. C. and Storm, B.: MIKE SHE. In: Singh VP (ed) Computer models of watershed hydrology, Highlands Ranch, Water Research Pub, Colorado, 1995.

Richards L. A.: Capillary conduction of liquids through porous medium, Physics, 1 (5): 318-333, Bibcode:1931Physi…1..318R. https://doi.org/10.1063/1.1745010, 1931.

Rozemeijer, J. C., Visser, A., Borren, W., Winegram, M., van der Velde, Y., Klein, J., and Broers, H. P.: High-frequency monitoring of water fluxes and nutrient loads to assess the effects of controlled drainage on water storage and nutrient transport, Hydrol. Earth Syst. Sci., 20, 347-358, https://doi.org/10.5194/hess-20-347-2016, 2016.

Rust, W., Holman, I., Bloomfield, J. Cuthbert, M., and Corstanje, R.: Understanding the potential of climate teleconnections to project future groundwater drought, Hydrol. Earth Syst. Sci., 23, 3233-3245, https://doi.org/10.5194/hess-23-3233-2019, 2019.

Ruttenberg, K.: The global phosphorus cycle. In Biochemistry, Vol. 8, treatiseon geochemistry, Schlesinger W (ed) (eds. H. Holland and K. Turekian). Elsevier-Pergamon: Oxford; 585-643, 2005.

Searcy, J. and Hardison, C. H.: Double –Mass Curves. Manual of Hydrology: Part 1, General Surface-Water Techniques, Geological Survey Water-Supply Paper 1541-B, 1960.

Schindler, D. W.: Recent advances in the understanding and management of eutrophication, Limnol. Oceanogr., 51, 356-363, https://doi.org/10.4319/lo.2006.51.1_part_2.0356, 2006.

Sharpley, A. N., Hedley, M. J., Sibbesen, E., Hillbricht-Ilkowska, A., House, W. A., and Ryszkowski, L.: Phosphorus transfer from terrestrial to aquatic ecosystems, In Phosphorus in the global environment, Tiessen H (ed), Scientific Committee on Problems of the Environment (SCOPE). John Wiley & SonsLtd.: Chichester; 171-199, 1995.

Simunek J., van Genuchten M. Th., and Sejna M.: The HYDRUS Software Package for Simulating Two- and Three-Dimensional Moovement of Water, Heat and Multiple Solutes in Variably-Saturated Media, Technical Manual, Version 2.0, PC Progress, Prague, Czech Republic, pp. 258, 2011.

Skaggs, R. W.: A water management model for shallow water table soils, University of North Carolina, Water Resource Research Institute, Technical Report 134, 1978.

Skaggs, R. W.: Combination surface-subsurface drainage systems for humid regions. J. Irrig. Drain. Div., ASCE. 106(IR4), 265-283, 1980a.

Skaggs, R. W.: Drainmod Reference Report, Methods for Design and Evaluation of Drainage-Water Management Systems for Soils with High Water Tables, U.S. Department of Agriculture, Soil Conservation Service, North Carolina State University, Raleigh, North Carolina, 1980b.

Skaggs, R. W., Wells, L. G., and Ghate, S. R.: Predicted and measured drainable porosities for field soils, Trans. ASAE, 21(3), 522-528, https://uknowledge.uky.edu/bae_facpub/199, 1978.

Skaggs, R. W., Youssef, M. A., and Chescheir, G. M.: DRAINMOD: Model Use, Calibration, and Validation, Trans. ASABE, 55(4), 1509-1522, https://doi.org/10.13031/2013.42259, 2012.

Smedema, L. K., Vlotman, W. F., and Rycroft, D.: Modern land Drainage. Planning, design and management of agricultural drainage systems, London: Taylor &Francis. https://doi.org/10.1201/9781003, 2004.

Smith, D. R., King, K. W., Johnson, L., Francesconi, W., Richards, P., Baker, D., and Sharpley, A. N.: Surface runoff and tile drainage transport of phosphorus in the Midwestern United States, J. Environ. Qual., 44, 495-502, https://doi.org/10.2134/jeq2014.04.0176, 2015.

Tomer, M. D., Meek, D. W., Jaynes, D. B., and Hatfield, J. L.: Evaluation of nitrate nitrogen fluxes from a tile-drained watershed in Central Iowa, J. Environ. Qual., 32, 642-653, https://doi.org/10.2134/jeq2003.6420, 2003.

Twarakavi, N. K. C., Sakai, M., and Simunek, J.: An objective analysis of the dynamic nature of field capacity, Water Resour. Res., 45, W10410, https://doi.org/10.1029/2009WR007944, 2009.

Van Esbroeck, C. J., Macrae, M. L., Brunke, R. I., and McKague, K.: Annual and seasonal phosphorus export in surface runoff and tile drainage from agricultural fields with cold temperate climates, J. Great Lakes Res., 42(6), 1271-1280, https://doi.org/10.1016/j.jglr.2015.12.014, 2016.

Van Esbroeck, C. J., Macrae, M. L., Brunke, R. R., and McKague, K.: Surface and subsurface phosphorus export from agricultural fields during peak flow events over the nongrowing season in regions with cool, temperate climates, Journal of Soil and Water Conservation, 72(1), 65-76, https://doi:10.2489/jswc.72.1.65 , 2017.

Van Schilfgaarde, J.: Nonsteady flow to drains, In *Drainage for Agriculture*, J. van Schilfgaarde, ed. American Society of Agronomy, Madison, W1. PP 245-270, 1974.

Vaughan, P. J., Suarez, D. L., Simunek, J., Corwin, D. L., and Rhoades, J. D.: Role of Groundwater Flow in Tile Drain Discharge, J. Environ. Qual., 28, 403-410, https://doi.org/10.2134/jeq1999.00472425002800020006x, 1999.

Vidon, P. and Cuadra, P. E.: Impact of precipitation characteristics on soil hydrology in tile drained landscapes, Hydrol. Process., 24, 1821-1833, https://doi.org/10.1002/hyp.7627, 2010.

Vivekananthan, K.: Environmental and Economic Consequences of Tile Drainage Systems in Canada, The Canadian Agri-Food Policy Institute, www.capi-icpa.ca, 2019.

Vivekananthan, K., Macrae, M., Lobb, D. A., and Ali, G. A.: Contribution of overland and tile flow to runoff and nutrient losses from vertisols in Manitoba, Canada, J. Environ. Qual., 48(4), 959-965, https://doi.org/10.2134/jeq2019.03.0103, 2019.

Waichler, S. R. and Wigmosta, M. S.: Development of Hourly Meteorological Values from Daily Data and Significance to Hydrological Modeling at H. J. Andrews Experimental Forest, Am. Meteorol. Soc., 4, 251-263, https://doi.org/10.1175/1525-7541(2003)4<251:DOHMVF>2.0.CO;2, 2003.

Williams, M. R., King, K. W., and Fausey, N. R.: Drainage water management effects on tile discharge and water quality, Agric. Water Manag., 148, 43-51, http://dx.doi.org/10.1016/j.agwat.2014.09.017, 2015.

Williams, M. R., King, K. W., Ford, W., Buda, A. R., and Kennedy, C. D.: Effect of tillage on macropore flow and phosphorus transport to tile drains, Water Resour. Res., 52, 2868-2882, https://doi.org/10.1002/2015WR017650, 2016.

Williams, M. R., Livingston, S. J., Heathman, G. C., and McAfee, S. J.: Thresholds for run-off generation in a drained closed depression, Hydrol. Process., 1-14, https://doi.org/10.1002/hyp.13477, 2019.

Youngs, E. G.: Effect of the Capillary fringe on Steady-State Water Tables in drained Lands, J. Irrig. Drain. Eng., 138(9), 809-814, https://doi.org/10.1061/(ASCE)IR.1943-4774.0000467, 2012.

Appendix A

Table A1. Instrument names and descriptions

Instrument name	**Description**
Hach Flo-tote and FL900 logger	Flow velocity and water level measurement
U20, Onset Ltd.	Barometrically-corrected pressure transducer
Temperature Smart Sensor S-THB-M002	Air temperature measurement
Wind Smart Sensor S-WSET-M002	Wind speed measurement
(Silicon Pyranometer)-S-LIB-M003	Solar radiation sensor
Tipping bucketrain gauge, 0.2 mm Rainfall Smart Sensor – SRGB-M002	Rainfall measurement
RH Smart Sensor(S-THB-M002)	Relative Humidity measurement

Appendix B

Table B1. Parameter names and their symbols in CRHM platform

Parameter symbol	**Parameter name**
Tair	Air temperature

Wspeed	Wind speed
RH	Relative Humidity
Qsi	Incoming solar irradiance
R	Rainfall
WQ_soil	Water Quality soil module
WT	Water table elevation above the semipermeable layer
SSS	Soil saturated storage or the saturated part of the soil moisture
soil_moist	Soil moisture
Poro_soil	Soil porosity
AL	Above layer
BL	Below layer
GWRD	Groundwater level fluctuations, groundwater recharge and discharge

Appendix C

Here, it was shown how seasonal factors ($f_{y,i}$) is assessed for different years. Equation (4) can be written as:

$$G_{y,i} = G \times f_{y,i} \qquad \text{(C1)}$$

For each year (y), $f_{y,i}$ for the first ($f_{y,1}$) and second ($f_{y,2}$) part of the sine function (G) were assessed individually. It should be note that in first and second part of the sine function for each year G is larger than zero ($G \geq 0$) and smaller than zero ($G < 0$), respectively. G can be defined for the two parts as:

$$\begin{cases} if\ G \geq 0\ \ [i = 1\,]then\ f_{y,1} = x \\ if\ G < 0\ \ [i = 2\,]then\ f_{y,2} = y \end{cases} \quad \text{(C-2)}$$

G is the sine function representing the annual fluctuations in water table (WT/SSS) or it can be simply defined as the percolation rate (in mm hr^{-1}) of soil water to groundwater through lower semi-permeable layer. So, for n years there are $n \times 2\ f_{y,i}$ values. The default values for $f_{y,i}$ are 1 and the default values can be changed for each year and for first and second parts in each year independently. Calculated $G_{y,i}$ in each time step add or subtracted to or from the total soil moisture depend on its sign. The $f_{y,i}$ values for the sine function parameters are presented in Fig. C1. The verified sine function time series along with time series of temperature, precipitation and calculated evapotranspiration are shown in Fig. C1. In this figure it is obvious that in years 2012 and 2015 to 2017 the warm season amplitudes are larger. The ET values are happened more in the warm seasons (growing seasons). Also, the seasonal oscillation in sine function is very similar to the temperature general oscillations.

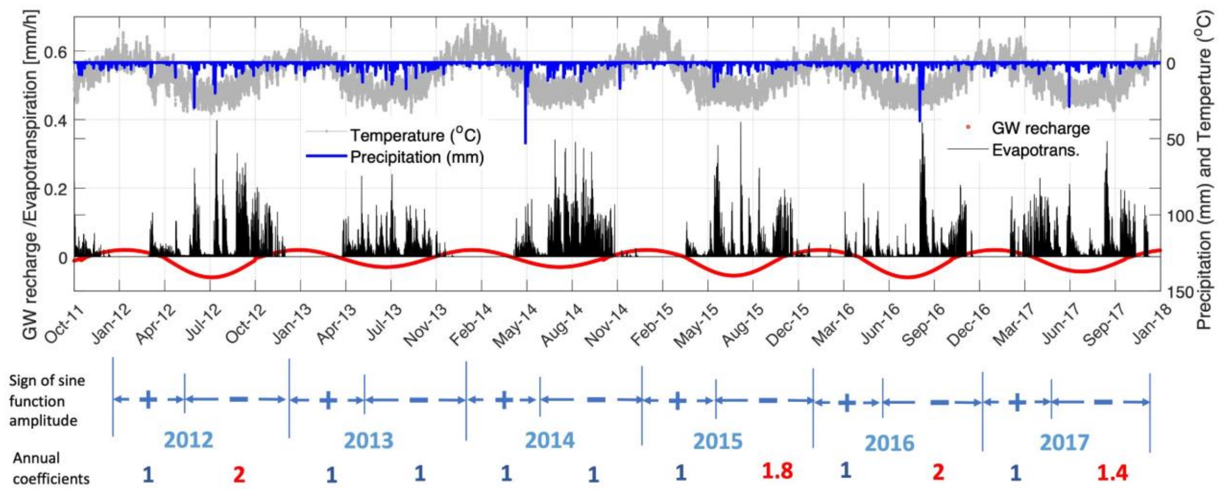

Figure C1. Time series of the adjustable sine function along with the time serioes of calculated evapotranspiration, temperature and precipitation during the study period from Oct 2011 to Sept 2018.

Appendix D

A sensitivity analysis was conducted for the cumulative tile flow (Q_{tc}), mean soil water table elevation (WT_m) and cumulative outflow rate from the semi-permeable layer at the bottom of the soil to groundwater (G_c) (see section 2.4.5, Eq. 4) with respect to six module parameters. Additionally, an approach for assessing model parameters at a new sites, potentially lacking water table elevation and tile flow observations is proposed.

D.1 Sensitivity analysis

In this section, the sensitivity of Q_{tc}, WT_m and G_c to six distinct module parameters, namely capillary fringe thickness (T_{CF}), capillary fringe drainable water (φ_c), soil saturated hydraulic conductivity (K), soil thickness (T_{SL}), sine function amplitude (A) and sine function (B) was examined. Q_{tc}, G_c and WT_m were computed over the entire simulation period, expressed in units of mm, mm and m, respectively. Figures D-1a to f illustrate these sensitivities, with each parameter's impact discussed in dedicated sections.

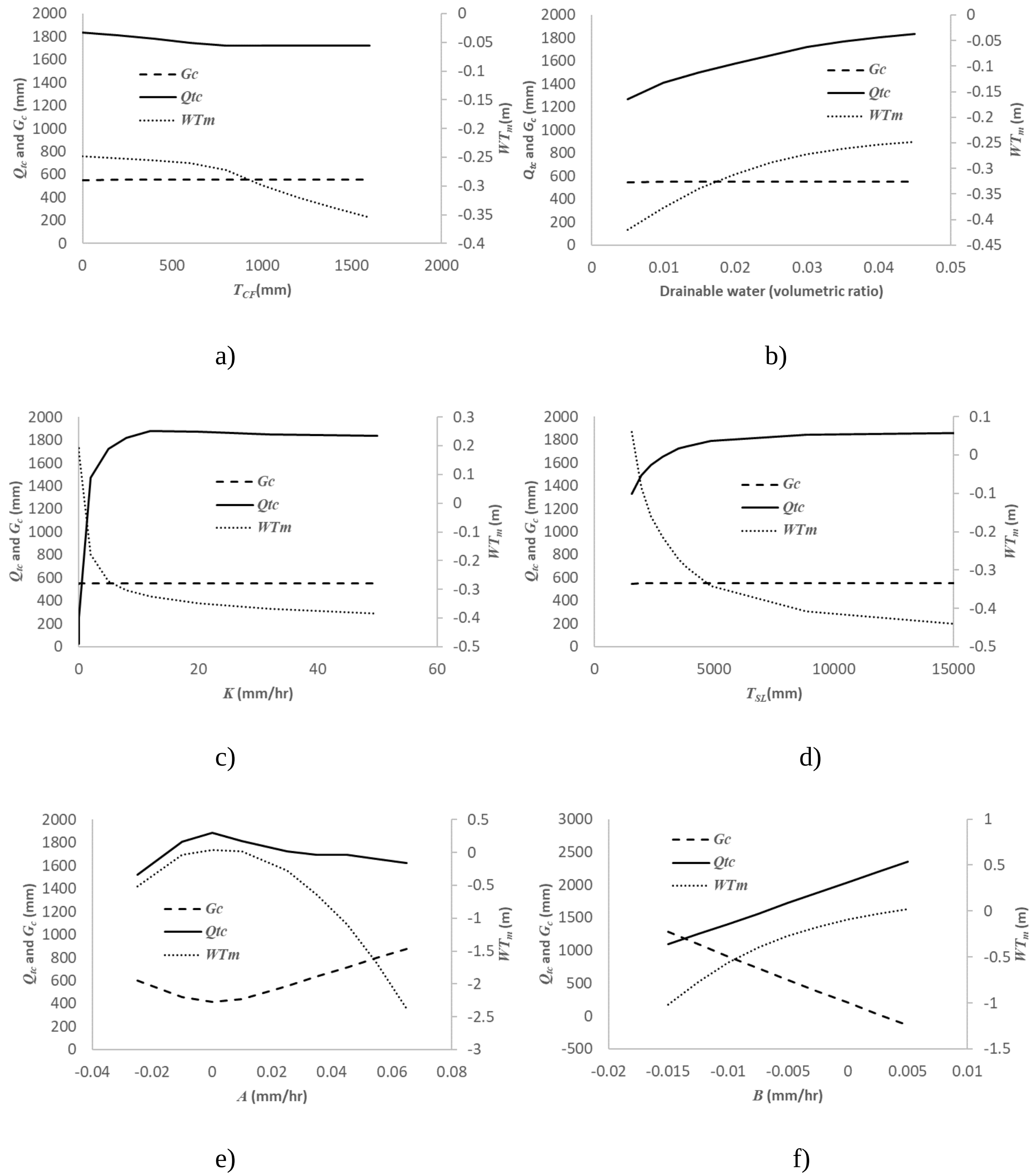

Figure D-1 Sensitivity of cumulative tile flow, Q_{tc}, cumulative soil to groundwater percolation rate, G_c, and mean soil water table elevation, WT_m, to capillary fringe thickness, T_{CF} (a) capillary fringe drainable water, φ_c (b), soil hydraulic conductivity, K (c), soil thickness, T_{SL} (d), sine function amplitude, A (e) and sine function intercept, B (f).

D.1.1 Sensitivity to capillary fringe thickness

To gauge sensitivity to capillary fringe thickness T_{CF}, flow rates and the WT_m were analyzed for T_{CF} ranging 0 to 1600 mm. Figure D-1a indicates that as T_{CF} increases, both cumulative tile flow (Q_{tc}) and mean soil water table (WT_m) decline. The WT_m drop is sharper for T_{CF} beyond 900 mm. Beyond this thickness, Q_{tc} stabilizes at a minimal value. A negative WT_m indicates its position below the tile pipe. G_c remains consistent despite T_{CF} variations.

D.1.2 Sensitivity to capillary fringe drainable water

With rising φ_c both Q_{tc} and WT_m surge (Figure D-1b). As φ_c ascends from 0.005 to 0.45, Q_{tc} jumps from 1300 mm to 1900 mm and WT_m from -0.45 m to -0.25 m (Figure D-1b). G_c stays constant, irrespective of φ_c fluctuations.

D.1.3 Sensitivity to soil hydraulic conductivity

Increasing soil hydraulic conductivity (K) from 0 to 10 mm hr^{-1}leads to a surge in Q_{tc} and a drop in WT_m (Figure D-1c). However, adjusting K from 10 to 50 mm hr^{-1} results in leveling off slopes for Q_{tc} and WT_m, especially when K> 20mm hr^{-1}. Both metrics are acutely responsive to K when K is below 10 mm hr^{-1} but become non-responsive beyond 20mm hr^{-1}. G_c's response to K remains neutral.

D.1.4 Sensitivity to soil thickness

Similar to K, a rise in T_{SL} from 1500mm to 15000 mm casue Q_{tc} to rise and WT_m to decline (Figure D-1d). The most significant rate of change for both metrics occurs between 1500 to 5000 mm T_{SL}. Beyond 5000 mm, changes flatten. G_c shows no response to T_{SL}variations.

D.1.5 Sensitivity to sine function amplitude

Increasing the sine function amplitude, A, from -0.03 to 0 mm hr^{-1} pushes both Q_{tc} and WT_m increase and reach to their maximum at A=0 (Figure D-1e). But as A rises from 0 to 0.06 mm hr^{-1}, they both decline. In contrast, G_c descends to its lowest (400 mm) when A shifts from -0.03 to 0 and then increases to 900 mm as A hits 0.063.

D.1.6 Sensitivity to sine function intercept

Both Q_{tc} and WT_m ascend with the growth in sine function's intercept, B. Increasing B from -0.015 to 0.005 mm hr^{-1}sees G_c descend. During this B increase, Q_{tc} expands from 1100 to 2400 mm, while G_c shrinks from 1400 to 0 mm. It seems the sum of Q_{tc} and G_c might be constant. This suggests that water either drains through the tile pipe or percolates through the soil bottom. Q_{tc}, and WT_m appear sensitive to all six module parameters, but G_c only to A and B.

D.2 Module parameter evaluation for new sites

As discussed in section 2.5, initial values for K, T_{CF} and φ_c can be determined by soil grain-size distribution. Parameters less explored in past research for new sites include the sine function's amplitude (A), intercept (B), and time delay (D_d).

D.2.1 Evaluating sine function's A and B

If no percolation exists from the soil's bottom to groundwater and $G_{y,i}$ is zero, both A and B should be zero. However, if percolation or interactions between soil and groundwater occurs, A and B need calibration assessment. Before this, reasonable initial values and bounds must be set. From this study's findings, A and B should fall between the mean hourly difference of infiltration and observed tile flow rates. For instance, observed hourly rates for infiltration and tile flow at our site are 0.07 and 0.03 mm hr^{-1}. Thus, A's and B's initial values should range from -0.04 to 0.04 mm hr^{-1}. Negative A and B values indicate outflow from soil to groundwater and vice versa. Initial values were set at 10% of the range limits: -0.004 for B and 0.004 for A. Eventually, B and A were adjusted to -0.005 and 0.025 mm hr^{-1}.

D.2.2 Assessment of sine function's time delay

The sine function begins on the first Julian day. If its peak occurs around 91st Julian day (three months later), its minimum should be on the 274th day. If the peak comes later, say the 111th day, a 20-day delay is present. This delay should mirror in both function's minima and maxima. In this case the minimum would be on day 294. This delay aligns with the soil water table's peak annual fluctuations. When no observed fluctuations exist, the delay can be calibrated. A sensible initial delay can be ascertained by examining the study site's water table elevations, fitting a sine function, and noting the peak's Julian day annually.